Calderón, C., Barrado, A., Rodríguez, A., Alou, P., Lázaro, A., Fernández, C., Zumel, P. (2018). General Analysis of Switching Modes in a Dual Active Bridge with Triple Phase Shift Modulation. *Energies,* 11 (9), 2419.

DOI: https://doi.org/10.3390/en11092419

energies

MDPI

Article

General Analysis of Switching Modes in a Dual Active Bridge with Triple Phase Shift Modulation

Carlos Calderon [1,*], Andres Barrado [1], Alba Rodriguez [1], Pedro Alou [2], Antonio Lazaro [1], Cristina Fernandez [1] and Pablo Zumel [1]

[1] Power Electronics System Group, Universidad Carlos III de Madrid, 28911 Leganes, Spain; barrado@ing.uc3m.es (A.B.); alba.rodriguez@uc3m.es (A.R.); alazaro@ing.uc3m.es (A.L.); cfernand@ing.uc3m.es (C.F.); pzumel@ing.uc3m.es (P.Z.)

[2] Centre of Industrial Electronics, Universidad Politecnica de Madrid, 28001 Madrid, Spain; pedro.alou@upm.es

* Correspondence: ccaldero@ing.uc3m.es; Tel.: +34-916-24-9188

Received: 11 August 2018; Accepted: 7 September 2018; Published: 12 September 2018

Abstract: This paper provides an exhaustive analysis of the Dual-Active-Bridge with Triple-Phase-Shift (DAB-TPS) modulation and other simpler ones, identifying all the possible switching modes to operate the DAB in both power flow directions, and for any input-to-output voltage range and output power. This study shows four cases and seven switching modes for each case when the energy flows in one direction. That means that the DAB operates up to fifty-six different switching modes when the energy flows in both directions. Analytical expressions for the inductor current, the output power, and the boundaries between switching modes are provided for all cases. Additionally, the combination of control variables to achieve Zero-Voltage-Switching (ZVS) or Zero-Current-Switching (ZCS) is provided for each case and switching mode, by showing which switching modes obtain ZVS or ZCS for the whole power range and all switches—independent of the input-to-output voltage ratio. Therefore, the most interesting cases, switching mode and modulation for using the DAB are identified. Additionally, experimental validation has been carried out with a 250 W prototype. This analysis is a proper tool to design the DAB in the optimum switching mode, reducing the RMS current and achieving to increase efficiency and the power density.

Keywords: Dual-Active-Bridge (DAB); soft switching; Triple-Phase-Shift (TPS); Single Phase-Shift; ZCS and ZVS

1. Introduction

Currently, the Dual-Active-Bridge (DAB) converter is commonly found in different sectors such as in electric vehicles, in which DAB converters are used as battery charges [1,2] or as active balancing systems [3]. The aeronautics industry is betting on improving emissions and reducing fuel consumption by replacing mechanical and pneumatic systems with electrical systems. In Reference [4] is shown a DAB working in harsh environments with high temperature as a component of an electric actuator; Reference [5] shows a DAB as an interface between the battery storage system and DC bus. Additionally, for electric ships [6,7] and smart grids [8–10], DAB converters can be seen as an interface component in the medium-voltage grid. DAB converters are also an alternative for electrochemical energy storage as shown in References [11,12].

The conventional DAB topology consists of two active bridges, a high-frequency transformer (T) and a series inductor (L)—Figure 1. The main characteristics of the DAB are bi-directionality, galvanic isolation, high power density, and soft switching in some operating conditions. Additionally, in the state-of-art, a variant of the DAB without transformer can be found, for application in mobile phones and computer chargers [13].

The most basic modulation applied to DAB is the Phase-Shift (PS), also known as Single-Phase-Shift (SPS), where simplicity its main advantage. In this case, it is only necessary to control the phase shift (φ) between the output voltage (v_{11} and v_{22}) of the bridges, with $D_1 = 1$ (pulse width of voltage v_{11}) and $D_2 = 1$ (pulse width of voltage v_{22})—Figure 2a. However, this kind of modulation has some disadvantages such as reduction of the operating range with Zero-Voltage-Switching (ZVS) or Zero-Current-Switching (ZCS), if the input-to-output voltage ratio moves away from the unity, and high currents at low power. Therefore, PS is not a proper modulation for wide output and input voltage ranges in the converter [14].

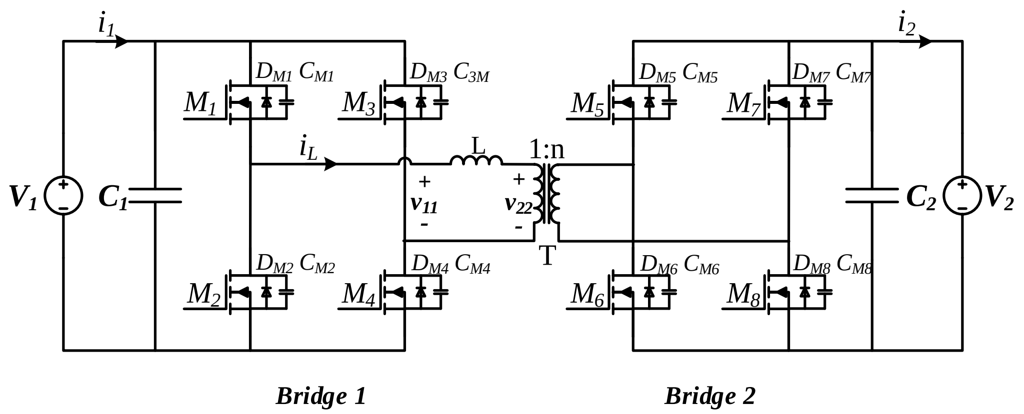

Figure 1. DAB Topology.

Another modulation scheme applied in DAB is the Extended-Phase-Shift modulation (EPS). This modulation operates by using the Phase-Shift (φ) between output voltages of the bridges, as in the PS modulation, along with the pulse width variation of the Bridge 1 output voltage (D_1), being $D_2 = 1$, Figure 2b. EPS modulation reduces the circulating energy and the conduction losses for medium power, therefore improving the performance compared to the PS modulation [15–19], although with a reduced impact for low power.

Additionally, with two degrees of freedom, the Dual-Phase-Shift modulation is well known (DPS) [20]. This modulation uses, once more, the Phase-Shift (φ) between output voltages of the bridges, as in the EPS modulation, along with the pulse width variation of both Bridges output voltages (D_1, D_2), in this case being $D_1 = D_2$, Figure 2c.

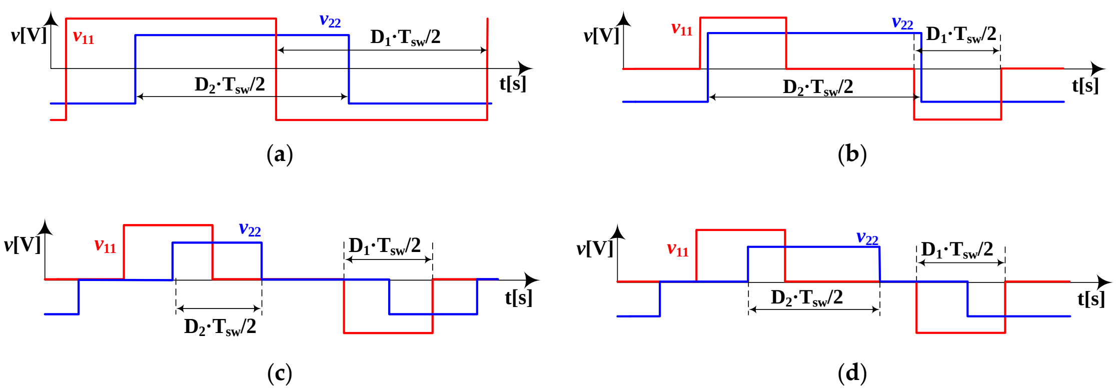

Figure 2. Types of modulation applied to Dual active bridge (DAB). (**a**) Phase shift (PS); (**b**) Extended phase shift (EPS); (**c**) Dual phase shift (DPS); and (**d**) Triple phase shift (TPS).

A more enhanced alternative is Triple-Phase-Shift modulation (TPS), which involves three control variables: The pulse width of the output voltages of Bridge 1 (D_1) and Bridge 2 (D_2), and the phase shift (φ) between both voltage waveforms, Figure 2d. This modulation strategy improves the converter's performances, with a more significant impact at low power, reduces RMS current, and presents a higher probability of soft switching operation [21–23]. However, the complexity increases due to the higher number of parameters to be controlled, which results in a higher number of possible switching modes of the converter [24–28]. There are different combinations of the three control variables that satisfy the same requirements of transferred power between the input and output ports of the converter. However, not all the combinations imply the same performance from switching conditions and circulating currents.

Many works can be found in the state-of-the-art that are focused on the study of the DAB switching modes, ZVS and ZCS operation, or RMS current reduction, among other topics. In References [26,27], the authors identify five switching modes (considering positives mismatches); in Reference [28], the number of switching modes increases to twelve (considering positive and negative mismatches), all of them for condition $V_1 > n \cdot V_2$. In Reference [29], the authors analyse the charge and discharge of the parasitic MOSFET capacitances to get ZVS. On the other hand, Reference [30] analyses the reduction of the transformer's coupling to achieve the same effect. However, all these works show useful partial solutions, but without doing a general analysis of all operation possibilities.

Therefore, the contribution of this paper is oriented to provide an exhaustive analysis of the different DAB switching modes when TPS, EPS, and PS modulation (DPS can be considered a particular case of TPS) are applied to get the best performance for whole output power range, and considering each V_1 and V_2 ratio (that includes buck and boost modes). Thanks to this in-depth analysis, the best switching modes are identified as well as the most combinations of the modulation variables to guarantee Zero-Voltage-Switching (ZVS) or Zero-Current-Switching (ZCS). This analysis is a tool to design the DAB converter, ensuring the soft-switching operation, and to improve the efficiency and the power density.

This paper organises as follows: Section 2 presents the basic operation of the TPS modulation applied to the DAB. Section 3 defines the Cases of study (based on bridges output voltages and their duty cycles) and the switching modes when TPS modulation is used, along with the inductor current expressions and the transmitted power for each switching mode. Section 4 analyses and calculates the expressions to get soft switching in the converter for each Case and switching mode. Section 5 validates the analysis for Case I and Case II with a 250 W prototype developed in the laboratory. Finally, Section 6 summarises the conclusions of the work carried out.

2. Triple-Phase-Shift Modulation

Triple-Phase-Shift (TPS) consists of shifting the driving signals v_{g3}, v_{g5} and v_{g7} with respect to v_{g1} (corresponding to the switches M_3, M_5, M_7, and M_1, respectively). By driving the switches in this way, v_{11} is generated at the output of the Bridge 1 of amplitude V_1, v_{22} is generated in the primary side of the transformer with an amplitude of V_2/n, and a current i_L flows through the inductor L.

Three control parameters define TPS modulation: D_1 ($0 < D_1 \leq 1$) representing the pulse width of voltage v_{11}, D_2 ($0 < D_2 \leq 1$) representing the pulse width of v_{22} and φ ($-\pi < \varphi < \pi$) measures the phase shift between v_{11} and v_{22}, as shown in Figure 3.

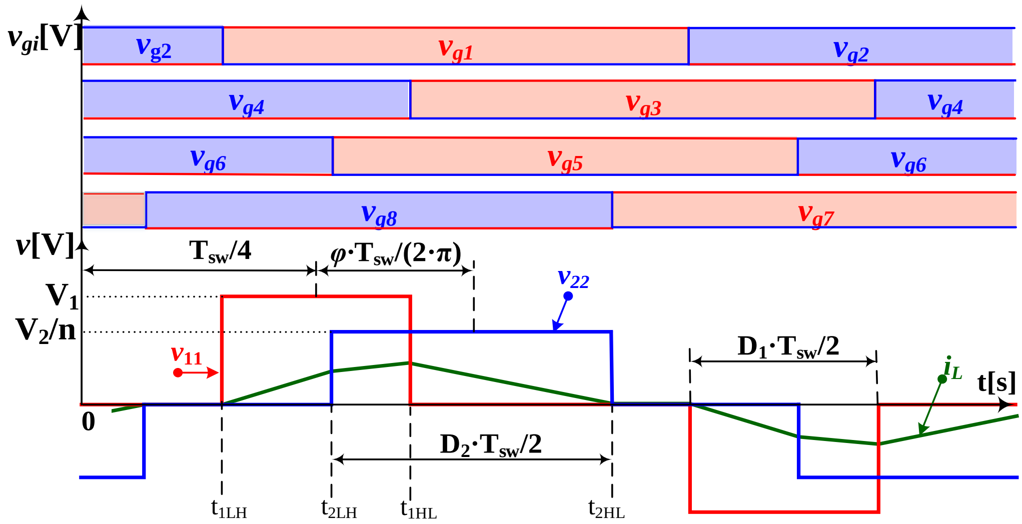

Figure 3. Typical voltages and current for a Dual active bridge (DAB) with a Triple phase shift (TPS) modulation.

The switching instants of the voltages v_{11} (t_{1LH} and t_{1HL}) and v_{22} (t_{2LH} and t_{2HL}), shown in Figure 3, are calculated by Equation (1), considering that the positive part of v_{11} centres in $T_{sw}/4$.

$$\begin{aligned} t_{1LH} &= \tfrac{T_{sw}}{2}\cdot\left(\tfrac{1}{2}-\tfrac{D_1}{2}\right) \\ t_{1HL} &= \tfrac{T_{sw}}{2}\cdot\left(\tfrac{1}{2}+\tfrac{D_1}{2}\right) \\ t_{2LH} &= \tfrac{T_{sw}}{2}\cdot\left(\tfrac{\varphi}{\pi}+\tfrac{1-D_2}{2}\right) \\ t_{2HL} &= \tfrac{T_{sw}}{2}\cdot\left(\tfrac{\varphi}{\pi}+\tfrac{1+D_2}{2}\right) \end{aligned} \quad (1)$$

3. Cases and Switching Modes

The switching modes define according to the profile acquired by the current i_L in each operating state. The current i_L is defined by the input parameters of the converter (V_1, V_2, n, L, f_{sw}) and by the parameters of the TPS modulation (D_1, D_2 and φ). By considering n, L and f_{sw} as constants, the voltages v_{11}, v_{22} and the pulse widths D_1 and D_2, four cases of study can be defined:

$$\text{Case I: } v_{11} \geq v_{22} \text{ and } D_1 > D_2$$

$$\text{Case II: } v_{11} \geq v_{22} \text{ and } D_1 \leq D_2$$

$$\text{Case III: } v_{11} < v_{22} \text{ and } D_1 > D_2$$

$$\text{Case VI: } v_{11} < v_{22} \text{ and } D_1 \leq D_2.$$

In Reference [20], the author concluded that the analysis performed for positive φ is equivalent to negative φ; therefore, DAB can operate in eight cases of study. Additionally, for positive φ, it can be observed that there are equivalences between Case I and Case IV, as well as between Case II and Case III; they obtain by exchanging v_{11} with v_{22}, and D_1 with D_2. It means that only the analysis of two of them is necessary. Therefore, in this paper, the analysis is developed for the Case I and II.

3.1. Switching Modes: Case I and Case II. Boundaries

The total switching modes per Case are seven: SM_1, SM_2, SM_2*, SM_3, SM_3*, SM_4, and SM_5; they can have positive or negative φ angle values (bidirectionality). Therefore, considering bi-directionality, four cases and seven switching modes per case, DAB can operate up to fifty-six switching modes. As aforementioned, Cases I and II are only analysed for positive φ angle values, as shown in Figures 4 and 5, respectively. These switching modes are obtained by increasing the phase shift φ for any value of D_1 and D_2.

The boundaries in each switching mode are obtained when the switching instants of the voltages v_{11} and v_{22} occur at the same time. For example, for SM_2 in Figure 4b: $t_{1HL} = t_{2HL}$ determines the lower boundary (switching mode from SM_1 to SM_2,) and the upper one when $t_{1HL} = t_{2LH}$ (switching mode from SM_2 to SM_3,), as shown in Equation (2).

$$\begin{aligned} \text{Lower boundary}: & \left(\frac{D_1 - D_2}{2}\right)\cdot\pi \\ \text{Upper boundary}: & \left(1 - \frac{D_1 + D_2}{2}\right)\cdot\pi \end{aligned} \tag{2}$$

The switching modes SM_2 and SM_3 are obtained for $D_1 < 1 - D_2$, whereas SM_2* and SM_3* are obtained for $D_1 \geq 1 - D_2$. The switching mode SM_2* is different concerning SM_2 only in the boundaries, whereas SM_3* is different regarding SM_3 in the boundaries, the current profile and the expression of the power, with respect to those in SM_3. Table 1 summarises the boundaries of all switching modes for Case I and Case II.

From the information in Table 1, the switching modes are plotted in a three-dimensional way depending on the parameters D_1, D_2 and φ, forming a cube with the unity side, as shown in Figure 6. The tetrahedral volumes contain the switching modes obtained with TPS modulation. In Case I: the modes SM_2 (DEFG), SM_2* (CEFG), SM_3* (BCEG) and SM_4 (ABEG), are shown in Figure 6a; and the modes SM_1 (CDEI), SM_3 (ADEG), and SM_5 (ABEH) are shown in Figure 6b. For Case II: the modes SM_2 (DFGJ), SM_2* (CFGJ), SM_3* (BCGJ), and SM_4 (ABGJ) are shown in Figure 6c; while, the modes SM_1 (CDJL), SM_3 (ADGJ), and SM_5 (ABJK), are shown in Figure 6d.

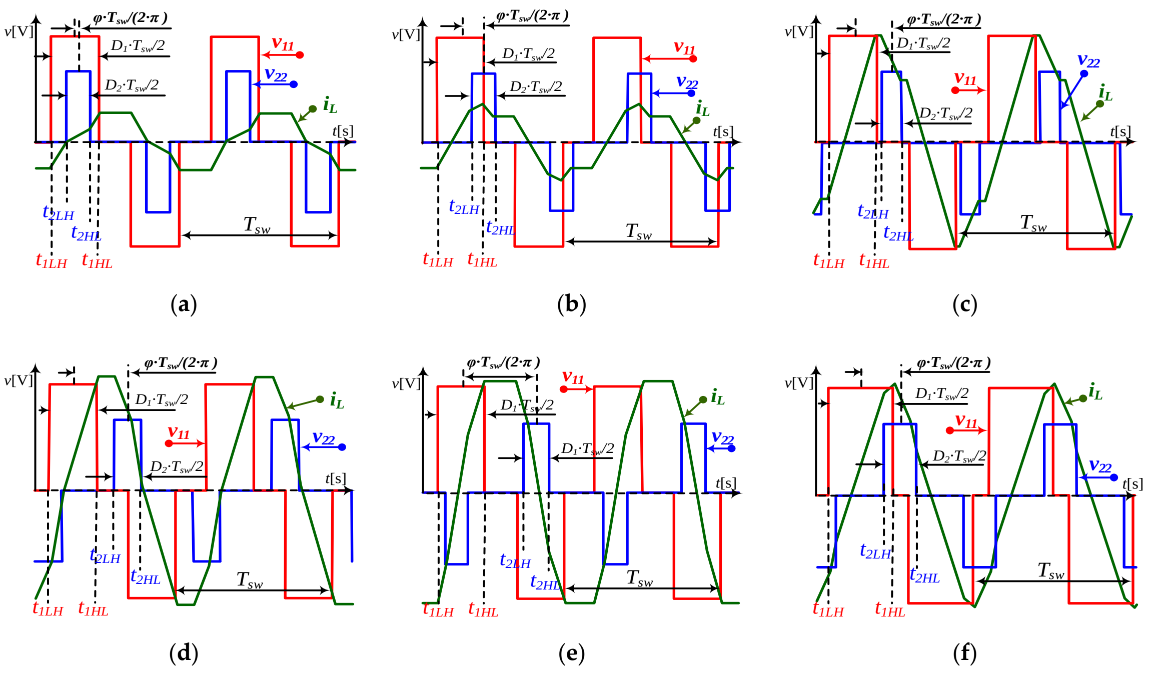

Figure 4. Case I: Switching modes for φ > 0. (**a**) SM_1; (**b**) SM_2, SM_2*; (**c**) SM_3; (**d**) SM_4; (**e**) SM_5, and (**f**) SM_3*.

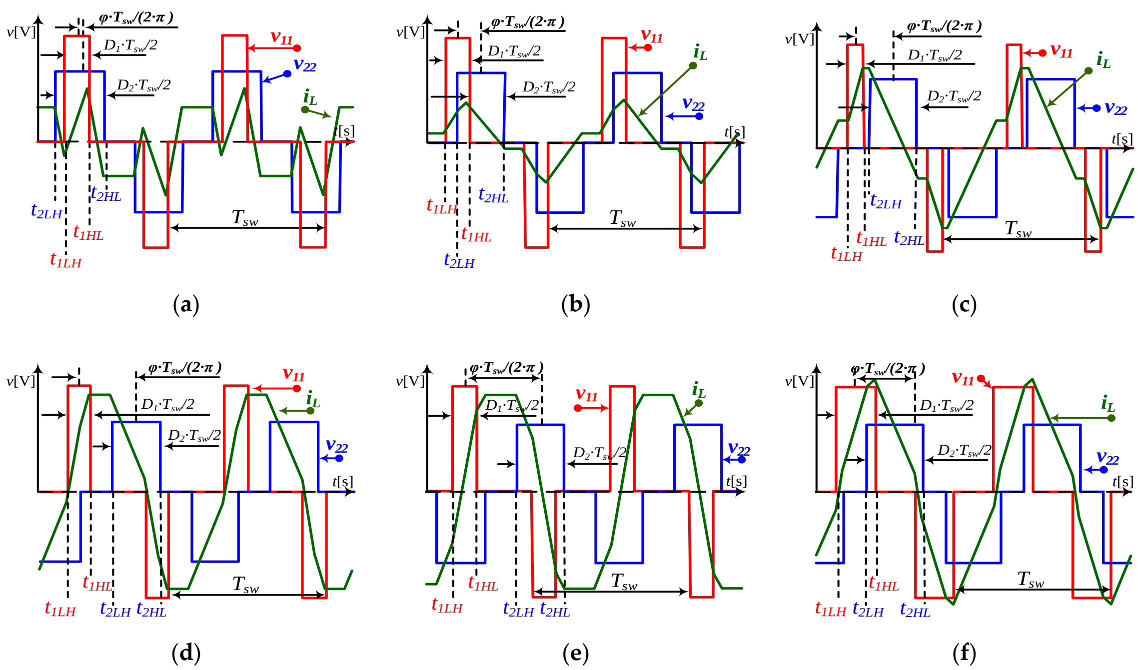

Figure 5. Case II: Switching modes for φ > 0. (**a**) SM_1; (**b**) SM_2, SM_2*; (**c**) SM_3; (**d**) SM_4; (**e**) SM_5, and (**f**) SM_3*.

Table 1. Boundaries for switching modes: Case I and Case II.

SM_i	Case I	Case II
SM_1	$0 < \varphi \leq \left(\frac{D_1-D_2}{2}\right)\cdot\pi$	$0 < \varphi \leq \left(\frac{D_2-D_1}{2}\right)\cdot\pi$
SM_2	$\left(\frac{D_1-D_2}{2}\right)\cdot\pi < \varphi \leq \left(\frac{D_1+D_2}{2}\right)\cdot\pi$	$\left(\frac{D_2-D_1}{2}\right)\cdot\pi < \varphi \leq \left(\frac{D_2+D_1}{2}\right)\cdot\pi$
SM_2*	$\left(\frac{D_1-D_2}{2}\right)\cdot\pi < \varphi \leq \left(1-\frac{D_1+D_2}{2}\right)\cdot\pi$	$\left(\frac{D_2-D_1}{2}\right)\cdot\pi < \varphi \leq \left(1-\frac{D_2+D_1}{2}\right)\cdot\pi$
SM_3	$\left(\frac{D_1+D_2}{2}\right)\cdot\pi < \varphi \leq \left(1-\frac{D_1+D_2}{2}\right)\cdot\pi$	$\left(\frac{D_2+D_1}{2}\right)\cdot\pi < \varphi \leq \left(1-\frac{D_2+D_1}{2}\right)\cdot\pi$
SM_3*	$\left(1-\frac{D_1+D_2}{2}\right)\cdot\pi < \varphi \leq \left(\frac{D_1+D_2}{2}\right)\cdot\pi$	$\left(1-\frac{D_2+D_1}{2}\right)\cdot\pi < \varphi \leq \left(\frac{D_2+D_1}{2}\right)\cdot\pi$
SM_4	$\left(1-\frac{D_1+D_2}{2}\right)\cdot\pi < \varphi \leq \left(1-\frac{D_1-D_2}{2}\right)\cdot\pi$	$\left(1-\frac{D_2+D_1}{2}\right)\cdot\pi < \varphi \leq \left(1-\frac{D_2-D_1}{2}\right)\cdot\pi$
SM_5	$\left(1-\frac{D_1-D_2}{2}\right)\cdot\pi < \varphi < \pi$	$\left(1-\frac{D_2-D_1}{2}\right)\cdot\pi < \varphi < \pi$

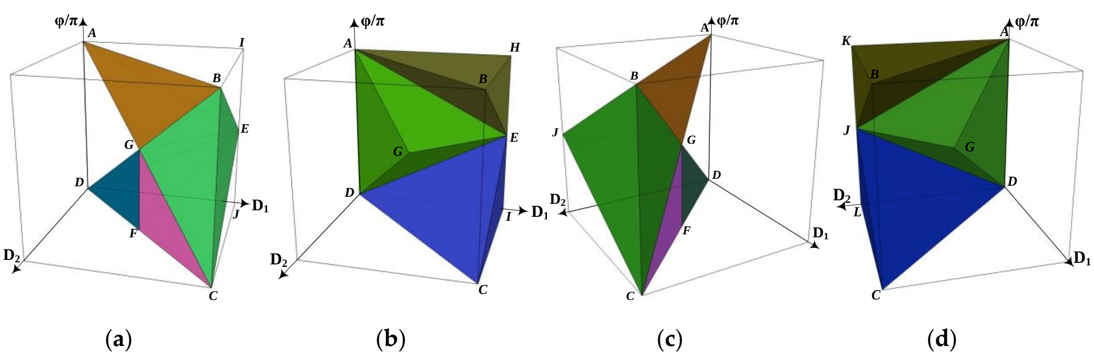

Figure 6. Switching modes. Case I: (**a**) SM_2, SM_2*, SM_3*, and SM_4; (**b**) SM_1, SM_3 and SM_5; Case II: (**c**) SM_2, SM_2*, SM_3*, and SM_4; and (**d**) SM_1, SM_3 and SM_5.

3.2. Current Through the Inductor L

The current i_L in each switching mode is calculated from Figure 4 (Case I) and Figure 5 (Case II), together with Equation (3) for four consecutive switching instants.

$$v_L = L\frac{di_L}{dt} \tag{3}$$

As an example, Figure 5a has t_{2LH}, t_{1LH}, t_{1HL} and t_{2HL} as consecutive switching instants and $i_L(t) = -i_L(t + T_{sw}/2)$; therefore, $i_L(t)$ must be calculated for half the switching period. Equation (4) shows $i_L(t)$ from t_{2LH} to t_{2HL} by applying Equation (3) and the equation systems in Equation (5) are obtained when switching instants are replaced in $i_L(t)$. Table 2, at Case II (column) and SM_1 (row), shows the solution of Equation (5).

$$i_L(t) = \begin{cases} i_L(t_{2LH}) - \frac{1}{L}\cdot\frac{V_2}{n}\cdot(t - t_{2LH});\ t_{2LH} \leq t < t_{1LH} \\ i_L(t_{1LH}) + \frac{1}{L}\cdot\left(V_1 - \frac{V_2}{n}\right)\cdot(t - t_{1LH});\ t_{1LH} \leq t < t_{1HL} \\ i_L(t_{1HL}) - \frac{1}{L}\cdot\frac{V_2}{n}\cdot(t - t_{1HL});\ t_{1HL} \leq t < t_{2HL} \end{cases} \tag{4}$$

$$\begin{array}{c} i_L(t_{1LH}) = i_L(t_{2LH}) - \frac{1}{L}\cdot\frac{V_2}{n}\cdot(t - t_{2LH}) \\ i_L(t_{1HL}) = i_L(t_{1LH}) + \frac{1}{L}\cdot\left(V_1 - \frac{V_2}{n}\right)\cdot(t - t_{1LH}) \\ i_L(t_{1HL}) = i_L(t_{1HL}) - \frac{1}{L}\cdot\frac{V_2}{n}\cdot(t - t_{1HL}) \\ i_L(t_{2HL}) = -i_L(t_{2LH}) \end{array} \tag{5}$$

Using the same procedure for each switching mode, Table 2 gathers the current i_L at the switching instant for Case I and Case II.

Table 2. Inductor current and output power for Case I and Case II.

SM_i	Current		Power	
	Case I	**Case II**	**Case I**	**Case II**
SM_1	$i_L(t_{1LH}) = -i_L(t_{1HL}) = -\frac{D_1 \cdot V_1 \cdot n - D_2 \cdot V_2}{4 \cdot L \cdot f_{sw} \cdot n}$ $i_L(t_{2LH}) = -\frac{D_2 \cdot V_1 \cdot n - 2 \cdot V_1 \cdot (\varphi/\pi) \cdot n - D_2 \cdot V_2}{4 \cdot L \cdot f_{sw} \cdot n}$ $i_L(t_{2HL}) = \frac{D_2 \cdot V_1 \cdot n + 2 \cdot V_1 \cdot (\varphi/\pi) \cdot n - D_2 \cdot V_2}{4 \cdot L \cdot f_{sw} \cdot n}$	$i_L(t_{1LH}) = -\frac{D_1 \cdot V_1 \cdot n - 2 \cdot V_2 \cdot (\varphi/\pi) - D_1 \cdot V_2}{4 \cdot L \cdot f_{sw} \cdot n}$ $i_L(t_{1HL}) = \frac{D_1 \cdot V_1 \cdot n + 2 \cdot V_2 \cdot (\varphi/\pi) - D_1 \cdot V_2}{4 \cdot L \cdot f_{sw} \cdot n}$ $i_L(t_{2HL}) = -i_L(t_{2LH}) = \frac{D_1 \cdot V_1 \cdot n - D_2 \cdot V_2}{4 \cdot L \cdot f_{sw} \cdot n}$	$\frac{V_1 \cdot V_2 \cdot D_2 \cdot (\varphi/\pi)}{2 \cdot L \cdot f_{sw} \cdot n}$	$\frac{V_1 \cdot V_2 \cdot D_1 \cdot (\varphi/\pi)}{2 \cdot L \cdot f_{sw} \cdot n}$
SM_2	$i_L(t_{1LH}) = -i_L(t_{2HL}) = -\frac{D_1 \cdot V_1 \cdot n - D_2 \cdot V_2}{4 \cdot L \cdot f_{sw} \cdot n}$ $i_L(t_{1HL}) = \frac{D_1 \cdot V_1 \cdot n + 2 \cdot V_2 \cdot \left(\frac{\varphi}{\pi}\right) - D_1 \cdot V_2}{4 \cdot L \cdot f_{sw} \cdot n}$ $i_L(t_{2LH}) = -\frac{D_2 \cdot V_1 \cdot n - 2 \cdot V_1 \cdot (\varphi/\pi) \cdot n - D_2 \cdot V_2}{4 \cdot L \cdot f_{sw} \cdot n}$		$\frac{V_1 \cdot V_2}{4 \cdot L \cdot f_{sw} \cdot n} \cdot \left[\frac{\varphi}{\pi} \cdot \left(D_1 + D_2 - \frac{\varphi}{\pi}\right) - \frac{(D_1 - D_2)^2}{4}\right]$	
SM_2^*				
SM_3	$i_L(t_{1LH}) = -i_L(t_{2HL}) = -\frac{D_1 \cdot V_1 \cdot n - D_2 \cdot V_2}{4 \cdot L \cdot f_{sw} \cdot n}$ $i_L(t_{1HL}) = i_L(t_{2LH}) = \frac{D_1 \cdot V_1 \cdot n + D_2 \cdot V_2}{4 \cdot L \cdot f_{sw} \cdot n}$		$\frac{V_1 \cdot V_2 \cdot D_1 \cdot D_2}{4 \cdot L \cdot f_{sw} \cdot n}$	
SM_3^*	$i_L(t_{1LH}) = -\frac{D_1 \cdot V_1 \cdot n + D_1 \cdot V_2 - 2 \cdot V_2 \cdot (1 - \varphi/\pi)}{4 \cdot L \cdot f_{sw} \cdot n}$ $i_L(t_{1HL}) = \frac{D_1 \cdot V_1 \cdot n - D_1 \cdot V_2 + 2 \cdot V_2 \cdot (\varphi/\pi)}{4 \cdot L \cdot f_{sw} \cdot n}$ $i_L(t_{2LH}) = -\frac{D_2 \cdot V_1 \cdot n - D_2 \cdot V_2 - 2 \cdot V_1 \cdot n \cdot (\varphi/\pi)}{4 \cdot L \cdot f_{sw} \cdot n}$ $i_L\left(t_{2HL} - \frac{T_{sw}}{2}\right) = -\frac{D_2 \cdot V_1 \cdot n + D_2 \cdot V_2 - 2 \cdot V_1 \cdot n \cdot (1 - \varphi/\pi)}{4 \cdot L \cdot f_{sw} \cdot n}$		$\frac{V_1 \cdot V_2}{2 \cdot L \cdot f_{sw} \cdot n} \cdot \left[\frac{\varphi}{\pi} \cdot \left(1 - \frac{\varphi}{\pi}\right) - \frac{(D_1 - 1)^2 + (D_2 - 1)^2}{4}\right]$	
SM_4	$i_L(t_{1LH}) = -\frac{D_1 \cdot V_1 \cdot n + D_1 \cdot V_2 - 2 \cdot V_2 \cdot (1 - \varphi/\pi)}{4 \cdot L \cdot f_{sw} \cdot n}$ $i_L(t_{1LH}) = i_L(t_{2LH}) = \frac{D_1 \cdot V_1 \cdot n + D_2 \cdot V_2}{4 \cdot L \cdot f_{sw} \cdot n}$ $i_L\left(t_{2HL} - \frac{T_{sw}}{2}\right) = \frac{D_2 \cdot V_1 \cdot n + D_2 \cdot V_2 - 2 \cdot V_1 \cdot n \cdot (1 - \varphi/\pi)}{4 \cdot L \cdot f_{sw} \cdot n}$		$\frac{V_1 \cdot V_2}{4 \cdot L \cdot f_{sw} \cdot n} \cdot \left[\left(1 - \frac{\varphi}{\pi}\right) \cdot \left(D_1 + D_2 + \frac{\varphi}{\pi} - 1\right) - \frac{(D_1 - D_2)^2}{4}\right]$	
SM_5	$i_L(t_{1LH}) = -i_L(t_{1HL}) = -\frac{D_1 \cdot V_1 \cdot n + D_2 \cdot V_2}{4 \cdot L \cdot f_{sw} \cdot n}$ $i_L\left(t_{2LH} - \frac{T_{sw}}{2}\right) = -\frac{D_2 \cdot V_1 \cdot n + D_2 \cdot V_2 + 2 \cdot V_1 \cdot n \cdot (1 - \varphi/\pi)}{4 \cdot L \cdot f_{sw} \cdot n}$ $i_L\left(t_{2HL} - \frac{T_{sw}}{2}\right) = \frac{D_2 \cdot V_1 \cdot n + D_2 \cdot V_2 - 2 \cdot V_1 \cdot n \cdot (1 - \varphi/\pi)}{4 \cdot L \cdot f_{sw} \cdot n}$	$i_L(t_{1LH}) = -\frac{D_1 \cdot V_1 \cdot n + D_1 \cdot V_2 - 2 \cdot V_2 \cdot \left(1 - \frac{\varphi}{\pi}\right)}{4 \cdot L \cdot f_{sw} \cdot n}$ $i_L(t_{1HL}) = \frac{D_1 \cdot V_1 \cdot n + D_1 \cdot V_2 + 2 \cdot V_2 \cdot \left(1 - \frac{\varphi}{\pi}\right)}{4 \cdot L \cdot f_{sw} \cdot n}$ $i_L\left(t_{2LH} - \frac{T_{sw}}{2}\right) = -i_L\left(t_{2HL} - \frac{T_{sw}}{2}\right)$ $= -\frac{D_1 \cdot V_1 \cdot n + D_2 \cdot V_2}{4 \cdot L \cdot f_{sw} \cdot n}$	$\frac{V_1 \cdot V_2 \cdot D_2 \cdot (1 - \varphi/\pi)}{2 \cdot L \cdot f_{sw} \cdot n}$	$\frac{V_1 \cdot V_2 \cdot D_1 \cdot (1 - \varphi/\pi)}{2 \cdot L \cdot f_{sw} \cdot n}$

3.3. Average Power

The input current, $i_1(t)$, is defined from t_{1LH} to t_{1HL} when the power is flowing to V_2. Without considering losses, the average power ($P = V_1 \cdot I_1$) is calculated by Equation (6) and i_L at the switching instant (Table 2). This average power is detailed for each switching mode in Table 2.

$$P = V_1 \cdot \frac{2}{T_{sw}} \int_{t_{1LH}}^{t_{1HL}} i_L(t)dt \tag{6}$$

4. Soft Switching

In general, soft switching is obtained either by Zero-Voltage-Switching (ZVS) or by Zero-Current-Switching (ZCS) of the converter switches. ZVS is achieved by switching on the switches M_1, M_4, M_6 and M_7 when $i_L < 0$, and in the switches M_2, M_3, M_5 and M_8 when $i_L > 0$. ZCS is achieved in all switches when $i_L = 0$, during switching-off. Table 3 describes, in detail, the soft switching conditions as a function of the current $i_L(t)$ for each switch in the converter.

For the sake of simplicity, the analysis described in this section is made without taking into account the parasitic inductances, capacitances, and resistances that are in real converters. In particular, MOSFET's parasitic capacitances that affect the soft switching conditions. The capacitances effect on the DAB has been previously analysed in several papers [26,31–33].

Table 3. Soft switching conditions for each switch.

Switch	ZVS	ZCS
M_1	$i_L(t_{1LH}) < 0$	$i_L(t_{1LH} + T_{sw}/2) = 0$
M_2	$i_L(t_{1LH} + T_{sw}/2) > 0$	$i_L(t_{1LH}) = 0$
M_3	$i_L(t_{1HL}) > 0$	$i_L(t_{1HL} + T_{sw}/2) = 0$
M_4	$i_L(t_{1HL} + T_{sw}/2) < 0$	$i_L(t_{1HL}) = 0$
M_5	$i_L(t_{2LH}) > 0$	$i_L(t_{2LH} + T_{sw}/2) = 0$
M_6	$i_L(t_{2LH} + T_{sw}/2) < 0$	$i_L(t_{2LH}) = 0$
M_7	$i_L(t_{2HL}) < 0$	$i_L(t_{2HL} + T_{sw}/2) = 0$
M_8	$i_L(t_{2HL} + T_{sw}/2) > 0$	$i_L(t_{2HL}) = 0$

4.1. Case I ($v_{11} \geq v_{22}$ and $D_1 > D_2$)

Table 4 is obtained by combining the current $i_L(t)$ through the inductor shown in Table 2 and the information in Table 3. Table 4 collects all the specific conditions to obtain ZVS or ZCS for all the switches in each switching mode for the Case I. ZCS is achieved when the equations are satisfied; ZVS is achieved when the inequalities are satisfied, for example: M_1 has ZVS when $(D_1 \cdot V_1 \cdot n > D_2 \cdot V_2)$ and ZCS $(D_1 \cdot V_1 \cdot n = D_2 \cdot V_2)$ for SM_1. Additionally, those conditions are classified into two types: depending on φ and non-depending on φ.

Table 4. Case I ($v_{11} \geq v_{22}$ and $D_1 > D_2$): General conditions to obtain Zero voltage switching (ZVS) and Zero current switching (ZCS) for each switch.

<table>
<tr><th rowspan="2">SM_i</th><th colspan="8">Switch</th></tr>
<tr><th>M_1</th><th>M_2</th><th>M_3</th><th>M_4</th><th>M_5</th><th>M_6</th><th>M_7</th><th>M_8</th></tr>
<tr><td>SM_1</td><td colspan="2" rowspan="4">$D_1 \cdot V_1 \cdot n \geq D_2 \cdot V_2$</td><td colspan="2">$D_1 \cdot V_1 \cdot n \geq D_2 \cdot V_2$</td><td colspan="2" rowspan="3">$\varphi \geq \left[\frac{D_2}{2} \cdot \left(1 - \frac{V_2}{V_1 \cdot n}\right)\right] \cdot \pi$</td><td colspan="2">$\varphi \leq -\left[\frac{D_2}{2} \cdot \left(1 - \frac{V_2}{V_1 \cdot n}\right)\right] \cdot \pi$</td></tr>
<tr><td>SM_2</td><td colspan="2" rowspan="2">$\varphi \geq \left[\frac{D_1}{2} \cdot \left(1 - \frac{V_1 \cdot n}{V_2}\right)\right] \cdot \pi$</td><td colspan="2" rowspan="3">$D_1 \cdot V_1 \cdot n \leq D_2 \cdot V_2$</td></tr>
<tr><td>SM_2*</td></tr>
<tr><td>SM_3</td><td colspan="2">$D_1 \cdot V_1 \cdot n + D_2 \cdot V_2 \geq 0$</td><td colspan="2">$D_1 \cdot V_1 \cdot n + D_2 \cdot V_2 \geq 0$</td></tr>
<tr><td>SM_3*</td><td colspan="2" rowspan="2">$\varphi \geq \left[1 - \frac{D_1}{2} \cdot \left(1 + \frac{V_1 \cdot n}{V_2}\right)\right] \cdot \pi$</td><td colspan="2">$\varphi \geq \left[\frac{D_1}{2} \cdot \left(1 - \frac{V_1 \cdot n}{V_2}\right)\right] \cdot \pi$</td><td colspan="2">$\varphi \geq \left[\frac{D_2}{2} \cdot \left(1 - \frac{V_2}{V_1 \cdot n}\right)\right] \cdot \pi$</td><td colspan="2" rowspan="3">$\varphi \geq \left[1 - \frac{D_2}{2} \cdot \left(1 + \frac{V_2}{V_1 \cdot n}\right)\right] \cdot \pi$</td></tr>
<tr><td>SM_4</td><td colspan="2" rowspan="2">$D_1 \cdot V_1 \cdot n + D_2 \cdot V_2 \geq 0$</td><td colspan="2">$D_1 \cdot V_1 \cdot n + D_2 \cdot V_2 \geq 0$</td></tr>
<tr><td>SM_5</td><td colspan="2">$D_1 \cdot V_1 \cdot n + D_2 \cdot V_2 \geq 0$</td><td colspan="2">$\varphi \leq \left[1 + \frac{D_2}{2} \cdot \left(1 + \frac{V_2}{V_1 \cdot n}\right)\right] \cdot \pi$</td></tr>
</table>

4.1.1. Non-Depending on φ

The non-depending on φ conditions (Table 4) summarise in the three expressions shown in Equation (7). The first condition ($D_1 \cdot V_1 \cdot n \geq D_2 \cdot V_2$) only fulfils when $D_1 \cdot V_1 \cdot n > D_2 \cdot V_2$ due to the Case I implies $v_{11} \geq v_{22}$ and $D_1 > D_2$. It means that switches with this condition have ZVS. However, the second condition ($D_1 \cdot V_1 \cdot n \leq D_2 \cdot V_2$) cannot be satisfied. Therefore, the switches depending on this condition switch with losses (Hard Switching). Finally, the last condition ($D_1 \cdot V_1 \cdot n + D_2 \cdot V_2 \geq 0$) can be satisfied for all the possible values of D_1, D_2 and n.

$$\begin{array}{c} D_1 \cdot V_1 \cdot n \geq V_2 \cdot D_2 \\ D_1 \cdot V_1 \cdot n \leq V_2 \cdot D_2 \\ D_1 \cdot V_1 \cdot n + V_2 \cdot D_2 \geq 0 \end{array} \tag{7}$$

4.1.2. Depending on φ

The conditions that depend on φ must be graphically analysed in a cube with the unity side. The switching mode SM_3* for the Case I is analysed, by considering the voltage ratio shown in Equation (8), to illustrate the procedure.

$$d = \frac{V_2}{n \cdot V_1} \tag{8}$$

Equation in (9) show soft switching conditions from Table 4 by considering Equation (8). The plane SS_{ij} (D_1, D_2) represents the soft switching conditions for "i" and "j" switches with any D_1 and D_2. Figure 6a and soft switching conditions in Equation (9) are plotted in Figure 7a for SM_3*. In Figure 7a, the switching mode SM_3* is represented by tetrahedron BCEG, and SS_{12} (D_1), SS_{34} (D_1), SS_{56} (D_2) and SS_{78} (D_2) are represented by the planes AKWX, DLYZ, DIUT, and AHTU, respectively.

Figure 7b–e show the projections of the soft switching conditions and SM_3* region onto the planes $\varphi/\pi - D_1$ and $\varphi/\pi - D_2$.

$$\begin{array}{c} SS_{12}\ (D_1, d) = \frac{\varphi}{\pi} = \left[1 - \frac{D_1}{2} \cdot \left(1 + \frac{1}{d}\right)\right] \ \forall\, D_2 \\ SS_{34}\ (D_1, d) = \frac{\varphi}{\pi} = \left[\frac{D_1}{2} \cdot \left(1 - \frac{1}{d}\right)\right] \ \forall\, D_2 \\ SS_{56}\ (D_2, d) = \frac{\varphi}{\pi} = \left[\frac{D_2}{2} \cdot (1 - d)\right] \ \forall\, D_1 \\ SS_{78}\ (D_2, d) = \frac{\varphi}{\pi} = \left[1 - \frac{D_2}{2} \cdot (1 + d)\right] \ \forall\, D_1 \end{array} \tag{9}$$

Figure 7b shows that M_1 and M_2 have soft switching for angles $\varphi/\pi \geq SS_{12}$ (D_1,d). It has been indicated by the region in which $\varphi/\pi \geq SS_{12}$ (D_1,d) (in grey), and the values D_1 and φ belonging to switching mode SM_3* (in green). All combination $D_1 - \varphi/\pi$, belonging to SM_3*, fulfil with $\varphi/\pi \geq SS_{12}$ (D_1,d), which means that both switches (M_1 and M_2) have soft switching for the entire operating range of SM_3*. The condition that allows having soft switching in the switches M_3 and M_4 fulfils if $\varphi/\pi \geq SS_{34}$ (D_1,d), Figure 7c. The condition SS_{34} (D_1,d) takes negative values for the range $0 < D_1 < 1$, this means that M_3 and M_4 always switch to soft switching for $\varphi/\pi > 0$.

Figure 7d shows that the projection of the tetrahedron belonging to SM_3* onto the $\varphi/\pi - D_2$ axes is the BCE plane. For the angles $\varphi/\pi = SS_{56}$ (D_2,d) and φ contained in the BCE triangle, ZCS is achieved in M_5 and M_6; on the other hand, when $\varphi/\pi > SS_{56}$ (D_2,d) and the BCE triangle contains to φ/π, M_5 and M_6 have ZVS. Similarly, switches M_5 and M_6, M_7 and M_8 have ZCS when $\varphi/\pi = SS_{78}$ (D_2,d) and ZVS for $\varphi/\pi > SS_{78}$ (D_2,d), and the BCE triangle contains to φ/π, Figure 7e. Finally, Figure 7f shows the values for D_1, D_2 and φ/π, in pink, that allow all the switches to have soft switching for SM_3*. From Figure 7f, it can be concluded that ZCS is only possible for switches M_7 and M_8 when the plane GTV contains to D_1, D_2 and φ/π; for the rest of the points belonging GBVT volume, all the switches have ZVS.

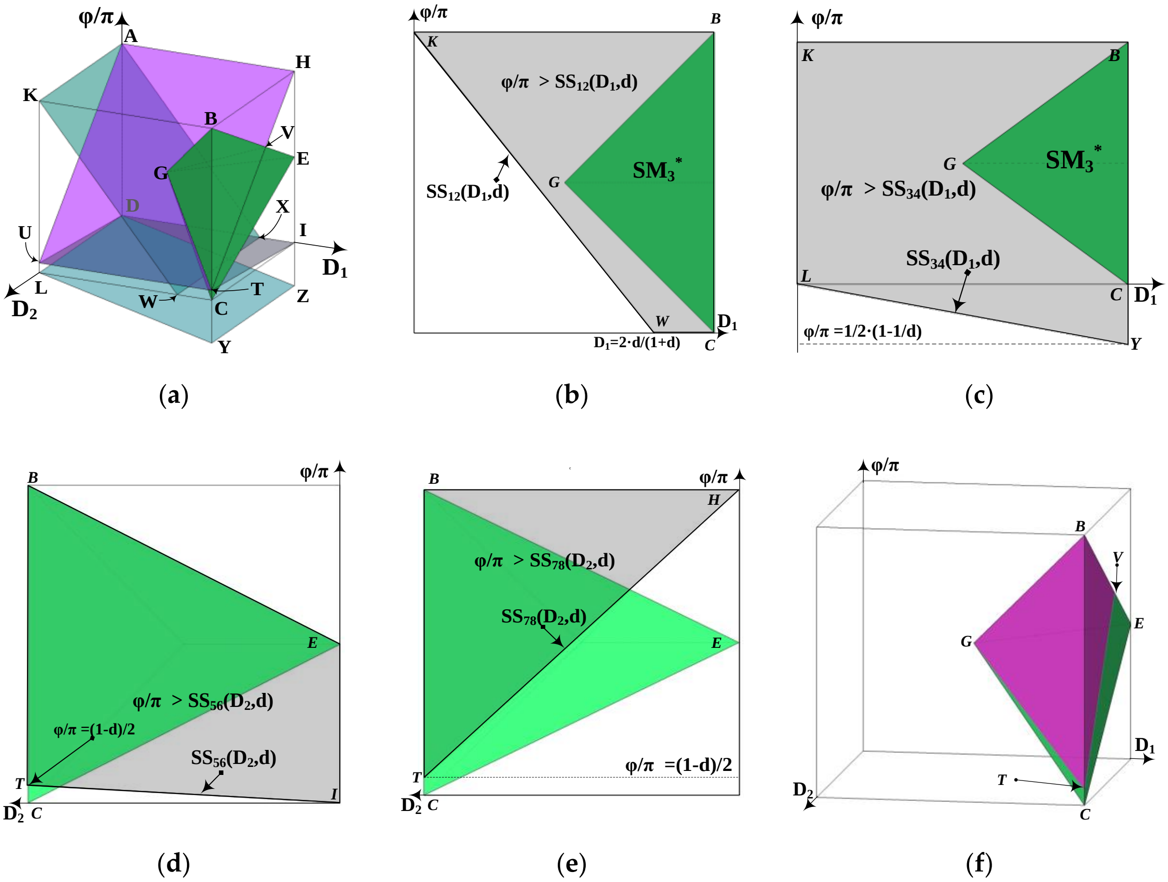

Figure 7. Case I (SM_3*): ZVS and ZCS Analysis. Projections of the soft switching conditions and SM_3* region onto the planes $\varphi/\pi - D1$ and $\varphi/\pi - D2$ (**a**) All soft switching conditions and SM_3* region; (**b**) Projections for M_1 and M_2; (**c**) Projections for M_3 and M_4; (**d**) Projections for M_5 and M_6; (**e**) Projections for M_7 and M_8; and (**f**) Soft switching region (BGTV) for all switches. For this case d = 0.677.

Table 5 summarises the type of turn on each switch for all switching modes, and the condition to get soft switching on the Bridge 2 switches.

Figure 8 shows the switching modes, power flow, RMS current through the inductor, and the boundary between HS and ZVS for M_5 to M_8 (conditions in Table 5) when D_1 takes different values (0.3, 0.6 and 0.95). Figure 8a,b depict the power flow and the RMS current for $D_1 = 0.3$ ($D_1 \leq 0.5$), and the switching modes SM_1, SM_2, SM_3, SM_4, and SM_5. For $D_1 = 0.6$ ($D_1 > 0.5$), two new switching modes appear, SM_2* and SM_3*, in the power flow, Figure 8c, and RMS current, Figure 8d. Finally, when $D_1 = 0.95$ both power flow, Figure 8e, and inductor RMS current, Figure 8f, tend to achieve the maximum levels. In short, higher power is obtained when D_1 is close to 1. For the same power flow, switching modes SM_1, SM_2, SM_2*, and SM_3* have less inductor RMS current than the rest of them, see Figure 8b,d,f. Soft switching in all switches, Table 5, is possible in SM_4, SM_5, and SM_3*, but SM_3* obtains the lowest inductor RMS current when $D_1 > 0.5$, Figure 8d,f. When $D_1 \leq 0.5$ less RMS currents appear in SM_1 and SM_2, see Figure 8b, but all switches in bridge 2 are in hard switching, see Table 5.

Table 5. Case I ($v_{11} \geq v_{22}$ and $D_1 > D_2$): Type of switching and conditions to obtain ZVS and ZCS for each switch.

<table>
<tr><th rowspan="2">SM_i</th><th rowspan="2">Range</th><th rowspan="2">Condition</th><th colspan="8">Type of Switching</th></tr>
<tr><th>M_1</th><th>M_2</th><th>M_3</th><th>M_4</th><th>M_5</th><th>M_6</th><th>M_7</th><th>M_8</th></tr>
<tr><td>SM_1</td><td>$0 < \varphi \leq \left(\frac{D_1 - D_2}{2}\right) \cdot \pi$</td><td rowspan="3">$SS_{56}\,(D_2, d) = \frac{D_2}{2} \cdot (1 - d)$</td><td colspan="2" rowspan="7">ZVS</td><td colspan="2" rowspan="7">ZVS</td><td colspan="2" rowspan="3">ZVS
$\varphi/\pi > SS_{56}\,(D_2,d)$
ZCS
$\varphi/\pi = SS_{56}\,(D_2,d)$
HS
$\varphi/\pi < SS_{56}\,(D_2,d)$</td><td colspan="2" rowspan="4">HS</td></tr>
<tr><td>SM_2</td><td>$\left(\frac{D_1 - D_2}{2}\right) \cdot \pi < \varphi \leq \left(\frac{D_1 + D_2}{2}\right) \cdot \pi$</td></tr>
<tr><td>SM_2*</td><td>$\left(\frac{D_1 - D_2}{2}\right) \cdot \pi < \varphi \leq \left(1 - \frac{D_1 + D_2}{2}\right) \cdot \pi$</td></tr>
<tr><td>SM_3</td><td>$\left(\frac{D_1 + D_2}{2}\right) \cdot \pi < \varphi \leq \left(1 - \frac{D_1 + D_2}{2}\right) \cdot \pi$</td><td>Always fulfil</td><td colspan="2">ZVS</td></tr>
<tr><td>SM_3*</td><td>$\left(1 - \frac{D_1 + D_2}{2}\right) \cdot \pi < \varphi \leq \left(\frac{D_1 + D_2}{2}\right) \cdot \pi$</td><td rowspan="3">$SS_{78}\,(D_2, d) = \left(1 - \frac{D_2}{2} \cdot (1 + d)\right)$</td><td colspan="2">ZVS
$\varphi/\pi > SS_{56}\,(D_2,d)$
ZCS
$\varphi/\pi = SS_{56}\,(D_2,d)$
HS
$\varphi/\pi < SS_{56}\,(D_2,d)$</td><td colspan="2" rowspan="3">ZVS
$\varphi/\pi > SS_{78}\,(D_2,d)$
ZCS
$\varphi/\pi = SS_{78}\,(D_2,d)$
HS
$\varphi/\pi < SS_{78}\,(D_2,d)$</td></tr>
<tr><td>SM_4</td><td>$\left(1 - \frac{D_1 + D_2}{2}\right) \cdot \pi < \varphi \leq \left(1 - \frac{D_1 - D_2}{2}\right) \cdot \pi$</td><td colspan="2" rowspan="2">ZVS</td></tr>
<tr><td>SM_5</td><td>$\left(1 - \frac{D_1 - D_2}{2}\right) \cdot \pi < \varphi < \pi$</td></tr>
</table>

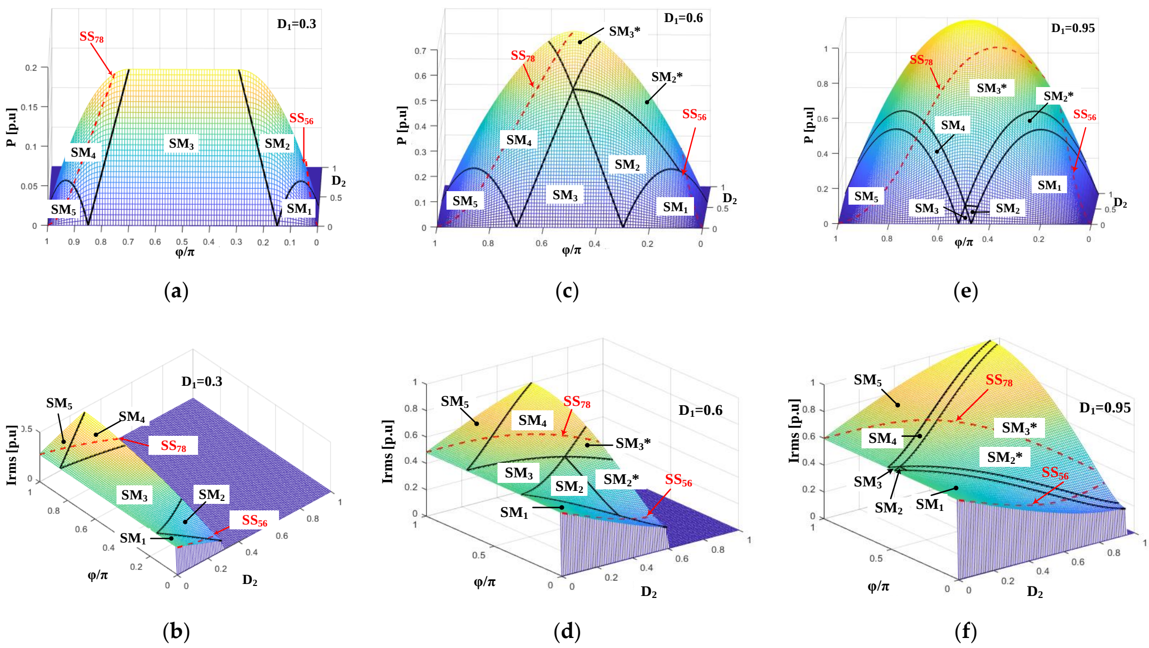

Figure 8. Case I: Power and RMS current per unit [p.u] normalized to the maximum values, and switching modes for different D_1 values when d = 0.677. (**a**) Power for $D_1 = 0.3$; (**b**) RMS current for $D_1 = 0.3$; (**c**) Power for $D_1 = 0.6$; (**d**) RMS current for $D_1 = 0.6$; (**e**) Power for $D_1 = 0.95$; and (**f**) RMS current for $D_1 = 0.95$.

4.2. Case II ($v_{11} \geq v_{22}$ and $D_1 \leq D_2$)

Similar to Case I, Table 6 summarises the conditions that allow the converter to have soft switching on all switches, considering positive φ. This table is equivalent to Table 4 for Case I. Again, there are two types of conditions that have soft switching: Those depending and those non-depending on φ.

Table 6. Case II ($v_{11} \geq v_{22}$ and $D_1 \leq D_2$): General conditions to obtain ZVS and ZCS for each switch.

<table>
<tr><th rowspan="2">SM_i</th><th colspan="4">Switch</th></tr>
<tr><th>M_1 M_2</th><th>M_3 M_4</th><th>M_5 M_6</th><th>M_7 M_8</th></tr>
<tr><td>SM_1</td><td>$\varphi \leq -\left[\frac{D_1}{2}\cdot\left(1-\frac{V_1 \cdot n}{V_2}\right)\right]\cdot\pi$</td><td rowspan="3">$\varphi \geq \left[\frac{D_1}{2}\cdot\left(1-\frac{V_1 \cdot n}{V_2}\right)\right]\cdot\pi$</td><td>$D_1 \cdot V_1 \cdot n \leq D_2 \cdot V_2$</td><td rowspan="4">$D_1 \cdot V_1 \cdot n \leq D_2 \cdot V_2$</td></tr>
<tr><td>SM_2</td><td rowspan="3">$D_1 \cdot V_1 \cdot n \geq D_2 \cdot V_2$</td><td rowspan="2">$\varphi \geq \left[\frac{D_2}{2}\cdot\left(1-\frac{V_2}{V_1 \cdot n}\right)\right]\cdot\pi$</td></tr>
<tr><td>SM_2*</td></tr>
<tr><td>SM_3</td><td>$D_1 \cdot V_1 \cdot n + D_2 \cdot V_2 \geq 0$</td><td>$D_1 \cdot V_1 \cdot n + D_2 \cdot V_2 \geq 0$</td></tr>
<tr><td>SM_3*</td><td rowspan="3">$\varphi \geq \left[1-\frac{D_1}{2}\cdot\left(1+\frac{V_1 \cdot n}{V_2}\right)\right]\cdot\pi$</td><td>$\varphi \geq \left[\frac{D_1}{2}\cdot\left(1-\frac{V_1 \cdot n}{V_2}\right)\right]\cdot\pi$</td><td>$\varphi \geq \left[\frac{D_2}{2}\cdot\left(1-\frac{V_2}{V_1 \cdot n}\right)\right]\cdot\pi$</td><td rowspan="2">$\varphi \geq \left[1-\frac{D_2}{2}\cdot\left(1+\frac{V_2}{V_1 \cdot n}\right)\right]\cdot\pi$</td></tr>
<tr><td>SM_4</td><td>$D_1 \cdot V_1 \cdot n + D_2 \cdot V_2 \geq 0$</td><td rowspan="2">$D_1 \cdot V_1 \cdot n + D_2 \cdot V_2 \geq 0$</td></tr>
<tr><td>SM_5</td><td>$\varphi \leq \left[1+\frac{D_1}{2}\cdot\left(1+\frac{V_1 \cdot n}{V_2}\right)\right]\cdot\pi$</td><td>$D_1 \cdot V_1 \cdot n + D_2 \cdot V_2 \geq 0$</td></tr>
</table>

4.2.1. Non-Depending on φ

As in Case I, the non-depending on φ conditions are shown in Equation (7), and all conditions could be fulfilled due to $V_1 \cdot n \geq V_2$ and $D_1 \leq D_2$, for Case II. So, from the first and the second conditions ($D_1 \cdot V_1 \cdot n \geq D_2 \cdot V_2$ and $D_1 \cdot V_1 \cdot n \leq D_2 \cdot V_2$) is obtained in Equation (10) as the only solution that meets both conditions at the same time, which means that the switches have ZCS. The third condition ($D_1 \cdot V_1 \cdot n + D_2 \cdot V_2 \geq 0$) always fulfils because all its parameters are always positive, which means that the corresponding switches achieve ZVS.

$$D_1 \cdot V_1 \cdot n = D_2 \cdot V_2 \tag{10}$$

The switching modes depicted in Figure 6c,d, for Case II, are simplified in Figure 9a when expression in Equation (10) is applied, turning the original volumes into planes. On the other hand, the application of the expression in Equation (10) implies a limitation to reach the maximum power in the converter due to the maximum value for D_1 = d, which is got when D_2 = 1. In order to reach the maximum power, the expression in Equation (10) has not been considered for d < D_1 < 1 and remaining as a constant D_2 = 1, as shown in Figure 9b. Note that the condition of this last interval coincides with the EPS modulation.

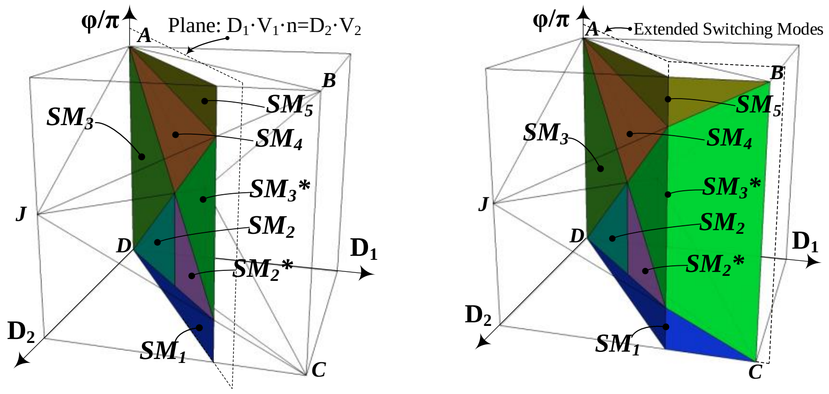

(**a**) (**b**)

Figure 9. Case II. Non-depending on φ conditions: (**a**) Switching modes for $D_1 \leq$ d; and (**b**) Extended Switching Modes for D_1 > d.

4.2.2. Depending on φ

Applying the expression in Equation (10), in Table 6, for 0 < $D_1 \leq$ d, the four conditions shown in Equation (11) summarise those that depend on φ.

$$
\begin{array}{c}
\varphi \geq -\left(\frac{D_2 - D_1}{2}\right)\cdot\pi \\
\varphi \leq \left(\frac{D_2 - D_1}{2}\right)\cdot\pi \\
\varphi \geq \left(1 - \frac{D_2 + D_1}{2}\right)\cdot\pi \\
\varphi \leq \left(1 + \frac{D_2 + D_1}{2}\right)\cdot\pi \\
\varphi \geq \left(\frac{D_2 - D_1}{2}\right)\cdot\pi
\end{array}
\quad (11)
$$

The first condition ($\varphi \geq -(D_2 - D_1)\cdot\pi/2$) indicates that the switches achieve soft switching when $\varphi \geq -(D_2 - D_1)\cdot\pi/2$. In Case II it is only possible to obtain ZVS for φ > 0 due to $D_1 \leq D_2$. The second condition means that ZVS is achieved when $0 < \varphi < (D_2 - D_1)\cdot\pi/2$, ZCS for $\varphi = (D_2 - D_1)\cdot\pi/2$ and HS in any other case. The third condition ($\varphi \geq (1 - (D_2 + D_1)/2)\cdot\pi$) indicates ZVS for $\varphi > (1 - (D_2 + D_1)/2)\cdot\pi$), ZCS for $\varphi = (1 - (D_2 + D_1)/2)\cdot\pi$) and HS for $\varphi < (1 - (D_2 + D_1)/2)\cdot\pi$). The fourth condition ($\varphi \leq (1 - (D_2 + D_1)/2)\cdot\pi$) indicates ZVS for φ < π, since for φ = π the output power is equal to zero. Finally, the fifth condition means that ZVS is achieved when $\varphi > (D_2 - D_1)\cdot\pi/2$, and ZCS for $\varphi = (D_2 - D_1)\cdot\pi/2$ and HS in any other case.

Therefore, by fulfilling expression in Equation (10), φ > 0 from first condition (lower boundary for SM_1, Table 1, Case II), up to $\varphi \leq (D_2 - D_1)\cdot\pi/2$ from the second condition (upper boundary for SM_1, Table 1, Case II), all switches for SM_1 get soft switching, see Table 6. By fulfilling expression in Equation (10) and $\varphi \geq (D_2 - D_1)\cdot\pi/2$ from the fifth condition (lower boundary for SM_2 and SM_2*, Table 1, Case II), all switches for SM_2 and SM_2* get soft switching. Only by fulfilling expression in Equation (10) do all switches for SM_3 get soft switching, see Table 6. In addition, by fulfilling expression in Equation (10) and $\varphi \geq (1 - (D_2 + D_1)/2)\cdot\pi$ from the third condition (lower boundary for SM_3*, Table 1, Case II), all switches for SM_3* get soft switching, see Table 6. By fulfilling expression in Equation (10) and $\varphi \geq (1 - (D_2 + D_1)/2)\cdot\pi$ from the third condition (lower boundary for SM_4, Table 1, Case II), all switches for SM_4 get soft switching. Finally, by fulfilling expression in Equation (10), $\varphi \geq (1 - (D_2 + D_1)/2)\cdot\pi$ from the third condition (φ values less than the lower boundary for SM_5, Table 1, Case II), and $\varphi < 1$ from the fourth condition, all switches for SM_5 get soft switching.

That means, for the simple fact of working in each switching mode, it would be fulfilling these conditions and having soft switching.

4.2.3. Extended Switching Modes

As said above, when analysing the non-depending on φ conditions, to overcome the limitation on the power delivered due to the early saturation of D_2, an additional condition that coincides with EPS modulation have to be considered. This operating zone is going to be called Extended Switching Mode, Figure 9b. The soft switching conditions in the Extended Switching Mode ($D_1 > d$ and $D_2 = 1$) are shown in Table 6, for the switching modes SM_1, SM_3* and SM_5. The boundaries of these three switching modes for the Extended Switching Mode are included in Table 7 and are shown in Figure 10a.

Additionally, soft switching conditions for the Extended Switching Mode are divided into those depending on φ and those non-depending on φ.

From Table 6 and $D_2 = 1$, the conditions that do not depend on φ are summarised in two equations, as shown in Equation (12). The first condition ($D_1 \leq d$) affects to SM_1, meaning that the switches M_5–M_8 for $D_1 > d$ lose the soft switching, see Figure 10b. The second condition ($D_1\cdot V_1\cdot n + D_2 \geq 0$) is always fulfilling, and only affects SM_5, which implies ZVS in switches M_5–M_8, see Figure 10b.

$$\begin{gathered} D_1 \leq d \\ D_1\cdot V_1\cdot n + D_2 \geq 0 \end{gathered} \tag{12}$$

Table 7. Case II ($v_{11} \geq v_{22}$ and $D_1 \leq D_2$): Boundaries for each extended switching modes.

SM_i	Case II
SM_1	$0 < \varphi \leq \left(\frac{1-D_1}{2}\right)\cdot\pi$
SM_3*	$\left(\frac{1-D_1}{2}\right)\cdot\pi < \varphi \leq \left(\frac{1+D_1}{2}\right)\cdot\pi$
SM_5	$\left(\frac{1+D_1}{2}\right)\cdot\pi < \varphi < \pi$

On the other hand, the depending on φ conditions for the same three switching modes (SM_1, SM_3* and SM_5), Table 6, are analysed similarly for $D_1 < d$. From Table 6 and considering Equation (8), for Case II $d \leq 1$ ($v_{22}/v_{11} = V_2/(n\cdot V_1) = d \leq 1$). For SM_1, the first condition ($\varphi \leq (-D_1/2\cdot(1 - 1/d))\cdot\pi$ or $\varphi \leq (D_1/2\cdot((1/d) - 1))\cdot\pi$) allows soft switching in M_1–M_2, line blue in Figure 10a, and the second condition ($\varphi \geq D_1/2\cdot(1 - 1/d)\cdot\pi$) is equivalent to consider $\varphi > 0$ due to $d \leq 1$, this means M_3–M_4 always have soft switching, see Figure 9a.

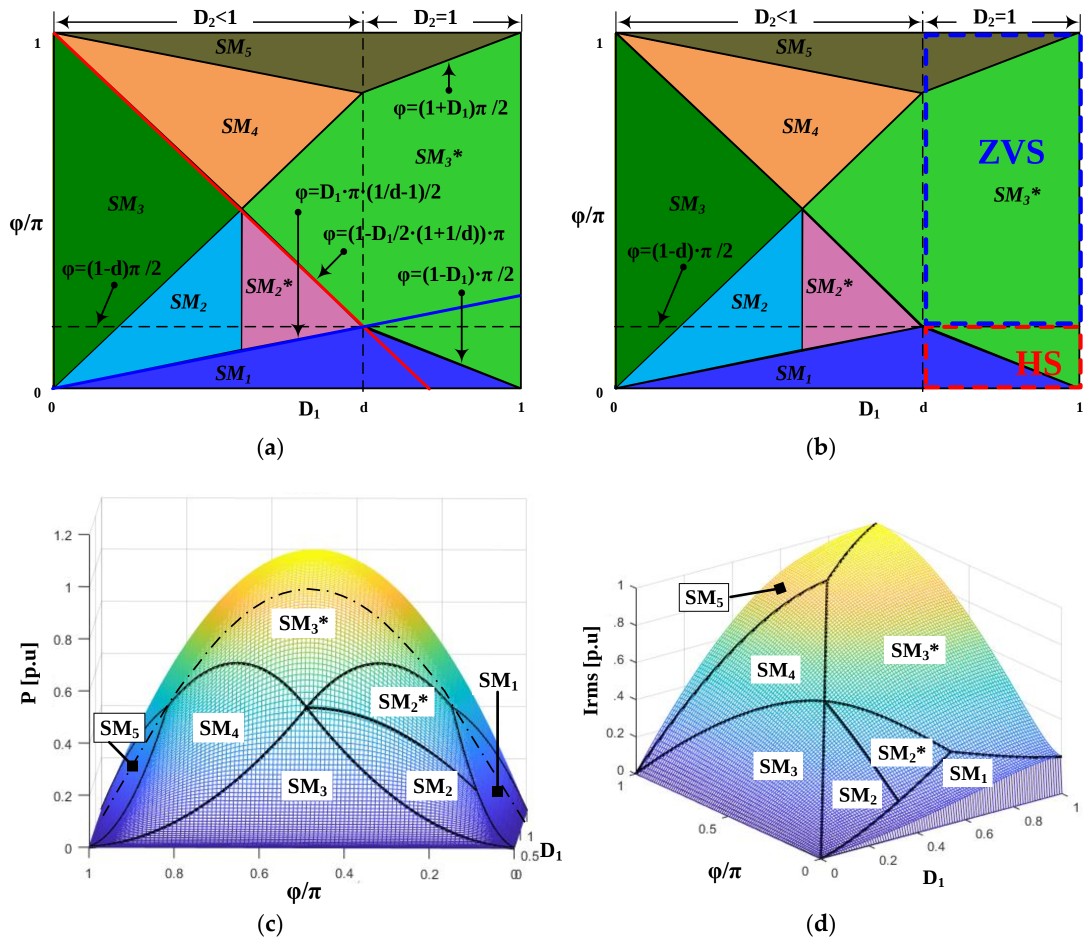

Figure 10. Case II for Extended Switching Modes (SM_1, SM_3*, SM_5), d = 0.677. (**a**) Depending and Non-depending soft switching conditions; (**b**) ZVS and hard switching (HS) zones; (**c**) Power flow [p.u]; and (**d**) Inductor RMS current [p.u]. [p.u] is normalized to the maximum values.

Soft switching conditions for SM_3* can be simplified as ($\varphi \geq (1 - D_1\cdot(1 + 1/d)/2)\cdot\pi$), ($\varphi \geq (D_1\cdot(1 - 1/d)\cdot\pi/2)$) and ($\varphi \geq (1 - d)\cdot\pi/2$), from Table 6; the third condition ($\varphi \geq (1 - D_1\cdot(1 + 1/d)/2)\cdot\pi$), red line in Figure 10a) indicates soft switching for M_1–M_2; the fourth condition ($\varphi \geq (D_1\cdot(1 - 1/d)/2)\cdot\pi$) is equivalent to $\varphi > 0$ due to $d \leq 1$, this means M_3–M_4 always have soft switching; and the fifth condition ($\varphi \geq (1 - d)\cdot\pi/2$, horizontal black dashed line in Figure 10a means soft switching for M_5–M_8.

Finally, soft switching conditions for SM_5 are ($\varphi \geq (1 - D_1\cdot(1 + 1/d)/2)\cdot\pi$) and ($\varphi \leq (1 + D_1\cdot(1 + 1/d)/2)\cdot\pi$); the sixth condition ($\varphi \geq (1 - D_1\cdot(1 + 1/d)/2)\cdot\pi$, red line, means soft switching for M_1–M_2, the seventh condition ($\varphi \leq (1 + D_1\cdot(1 + 1/d)/2)\cdot\pi$) is equivalent to $\varphi < \pi$ and it indicates soft switching for M_3–M_4, see Figure 10a.

Depending and non-depending soft switching conditions are summarised in Table 8 and Figure 10b for $D_1 > d$ and $D_2 = 1$. All the switches have zero voltage switching in the ZVS zone (blue dashed rectangle). For SM_1, M_1–M_2 always have hard switching; and for SM_3* and $\varphi < (1 - d)\cdot\pi/2$, M_5 to M_8, always have hard switching, see HS zone (red dashed rectangle). Table 8 shows the results of the analysis performed for Case II and shows the ranges of each switching mode, the power transferred and the type of switching in the switches.

Figure 10c,d shows the power flow and the inductor RMS current, respectively. As depicted, the lower RMS current can be obtained at the boundary between SM_1, SM_2 and SM_2*, compared with SM_3, SM_4 and SM_5 for the same transferred power.

Table 8. Case II (v11 $\geq$ v22 and D1 $\leq$ D2): Boundaries, power, and type of switching for each switch.

<table>
<tr><th colspan="2" rowspan="2">SM_i</th><th rowspan="2">Range</th><th rowspan="2">Power</th><th colspan="4">Type of Switching</th></tr>
<tr><th>M_1–M_2</th><th>M_3–M_4</th><th>M_5–M_6</th><th>M_7–M_8</th></tr>
<tr><td rowspan="8">$D_1 \leq d$
$D_2 = D_1/d$</td><td rowspan="2">SM_1</td><td>$0<\varphi<\frac{D_1\cdot(d-1)}{2\cdot d}\cdot\pi$</td><td rowspan="2">$\frac{V_1^2\cdot D_1^2\cdot\varphi}{2\cdot L\cdot f_{sw}\cdot D_2\cdot\pi}$</td><td>ZVS</td><td rowspan="8">ZVS</td><td rowspan="2">ZCS</td><td rowspan="5">ZCS</td></tr>
<tr><td>$\varphi=\frac{D_1\cdot(d-1)}{2\cdot d}\cdot\pi$</td><td rowspan="4">ZCS</td></tr>
<tr><td>SM_2</td><td>$\frac{D_1\cdot(d-1)}{2\cdot d}\cdot\pi<\varphi<\frac{D_1\cdot(d+1)}{2\cdot d}\cdot\pi$</td><td rowspan="2">$\frac{V_1^2\cdot d}{4\cdot L\cdot f_{sw}}\left[\frac{\varphi}{\pi}\cdot\left(\frac{D_1}{d}\cdot(d+1)-\frac{\varphi}{\pi}\right)-\frac{D_1^{\,2}\cdot(d-1)^2}{4\cdot d^2}\right]$</td><td rowspan="6">ZVS</td></tr>
<tr><td>SM_2*</td><td>$\frac{D_1\cdot(d-1)}{2\cdot d}\cdot\pi<\varphi<1-\frac{D_1\cdot(d+1)}{2\cdot d}\cdot\pi$</td></tr>
<tr><td>SM_3</td><td>$\frac{D_1\cdot(d+1)}{2\cdot d}\cdot\pi<\varphi<1-\frac{D_1\cdot(d+1)}{2\cdot d}\cdot\pi$</td><td>$\frac{V_1^2\cdot D_1^2}{4\cdot L\cdot f_{sw}}$</td></tr>
<tr><td>SM_3*</td><td>$\left(1-\frac{D_1\cdot(d+1)}{2\cdot d}\right)\cdot\pi<\varphi\leq\frac{D_1\cdot(d+1)}{2\cdot d}\cdot\pi$</td><td>$\frac{V_1^2\cdot d}{2\cdot L\cdot f_{sw}}\left[\frac{\varphi}{\pi}\cdot\left(1-\frac{\varphi}{\pi}\right)-\frac{(D_1-1)^2+(D_2-1)^2}{4}\right]$</td><td rowspan="3">ZVS</td><td rowspan="3">ZVS</td></tr>
<tr><td>SM_4</td><td>$\left(1-\frac{D_1\cdot(d+1)}{2\cdot d}\right)\cdot\pi<\varphi\leq\left(1-\frac{D_1\cdot(d-1)}{2\cdot d}\right)\cdot\pi$</td><td>$\frac{V_1^2\cdot d}{4\cdot L\cdot f_{sw}}\left[\left(1-\frac{\varphi}{\pi}\right)\cdot\left(\frac{D_1}{d}(d+1)+\frac{\varphi}{\pi}-1\right)-\frac{D_1^{\,2}(d-1)^2}{4\cdot d^2}\right]$</td></tr>
<tr><td>SM_5</td><td>$\left(1-\frac{D_1\cdot(d-1)}{2\cdot d}\right)\cdot\pi<\varphi\leq\pi$</td><td>$\frac{V_1^2\cdot D_1\cdot\left(1-\frac{\varphi}{\pi}\right)}{2\cdot L\cdot f_{sw}}$</td></tr>
<tr><td rowspan="5">$D_1 > d$
$D_2 = 1$</td><td>SM_1</td><td>$0<\varphi\leq\left(\frac{D_1-1}{2}\right)\cdot\pi$</td><td>$\frac{V_1^2\cdot D_1^2\cdot\varphi}{2\cdot L\cdot f_{sw}\cdot\pi}$</td><td rowspan="5">ZVS</td><td rowspan="5">ZVS</td><td rowspan="2">HS</td><td rowspan="2">HS</td></tr>
<tr><td rowspan="3">SM_3*</td><td>$\left(\frac{1-D_1}{2}\right)\cdot\pi<\varphi<\left(\frac{1-d}{2}\right)\cdot\pi$</td><td rowspan="3">$\frac{V_1^2\cdot d}{2\cdot L\cdot f_{sw}}\left[\frac{\varphi}{\pi}\cdot\left(1-\frac{\varphi}{\pi}\right)-\frac{(D_1-1)^2}{4}\right]$</td></tr>
<tr><td>$\varphi=\left(\frac{1-d}{2}\right)\cdot\pi$</td><td>ZCS</td><td>ZCS</td></tr>
<tr><td>$\left(\frac{1-d}{2}\right)\cdot\pi<\varphi<\left(\frac{1+D_1}{2}\right)\cdot\pi$</td><td rowspan="2">ZVS</td><td rowspan="2">ZVS</td></tr>
<tr><td>SM_5</td><td>$\left(\frac{3-D_1}{2}\right)\cdot\pi<\varphi\leq\pi$</td><td>$\frac{V_1^2\cdot D_1\cdot\left(1-\frac{\varphi}{\pi}\right)}{2\cdot L\cdot f_{sw}}$</td></tr>
</table>

5. Experimental Results

This section shows the experimental results for Case I and Case II using a 250 W prototype. The prototype has IRFP4468PbF MOSFETs in both bridges, a transformer built with an ETD59 ferrite core and a self-manufactured inductor with a RM12 ferrite core. Additionally, a TMS320F28335 Texas Instrument DSP generates the driving signals.

Table 9 summarises the operating parameters of the converter, and Figure 11 shows a block diagram of the experimental circuit layout.

Table 9. DAB parameters.

Descriptions	Specifications
Port 1 Voltage V_1	36 V
Port 2 Voltage V_2	72 V
Transformer turns ratio: 1:n	1:3
Inductance: L	3.88 µH
Switching frequency: f_{sw}	100 kHz
Port 1 capacitor: C_1	60 µF
Port 2 capacitor: C_2	60 µF

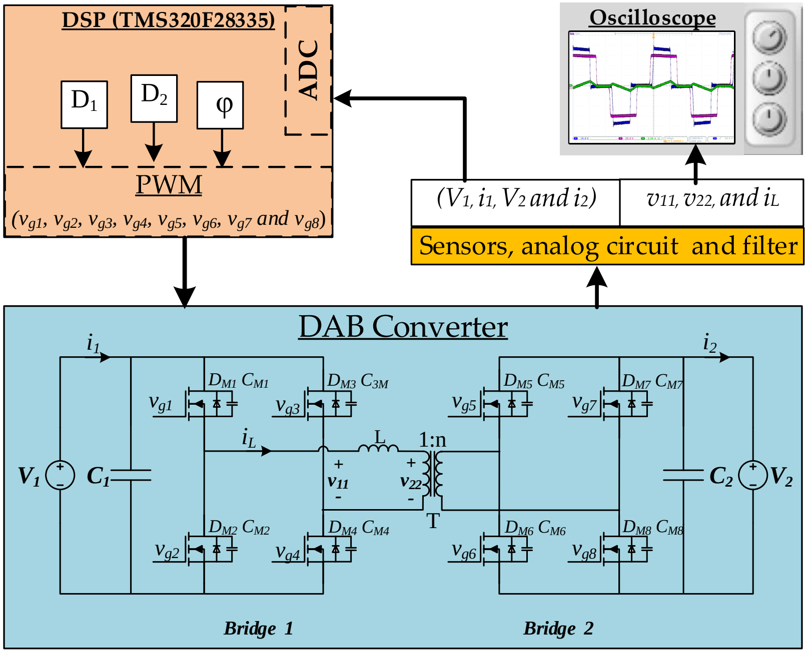

Figure 11. Block diagram of the experimental circuit layout.

Figure 12 shows six switching modes (SM_1, SM_2, SM_2*, SM_3*, SM_4, y SM_5) for Case I and d = 0.677, which validate the analysis performed about the switching types, detailed in Table 5. Figure 12a–c show ZVS in M_1, M_2, M_3, and M_4; HS in M_7 and M_8; and for M_5 and M_6 the switching type depend on φ and D_2. In Figure 12d–f, the switching type for M_7 and M_8 varies in function of φ and D_2, whereas the rest of switches maintain the same switching type (ZVS). Figure 12a shows the voltages v_{11}, v_{22} and i_L for the switching mode SM_1, in which the four switches of the Bridge 1 (M_1–M_4) are operating with ZVS. On Bridge 2, switches M_5 and M_6 switch with losses (HS) due to ($\varphi/\pi = 0.050$) < ($SS_{56} = 0.059$), as shown in Table 5, for $D_1 = 0.5$ and $D_2 = 0.34$. Switches M_7 and M_8 are in HS, as was specified in Table 5. In Figure 12b, the eight switches switch in the same way as shown in Figure 12a, for $D_1 = 0.5$, $D_2 = 0.45$ and ($\varphi/\pi = 0.061$) < ($SS_{56} = 0.075$). In the switching mode SM_2*, Figure 12c shows ZVS in M_5 and M_6 for ($\varphi/\pi = 0.222$) > ($SS_{56} = 0.077$) with $D_1 = 0.75$ and $D_2 = 0.487$. Figure 12d shows the switching mode SM_3* with ZVS in M_7 and M_8 when $D_1 = 0.75$, $D_2 = 0.643$ and ($\varphi/\pi = 0.577 \cdot \pi$) > ($SS_{78} = 0.494$). In Figure 12e, switches M_7 and M_8 achieve ZVS for $D_1 = 0.75$, $D_2 = 0.5$ and ($\varphi/\pi = 0.722$) > ($SS_{78} = 0.667$) in the switching mode SM_4. For the last switching mode, SM_5, the parameters $D_1 = 0.75$, $D_2 = 0.2$, and ($\varphi/\pi = 0.75$) < ($SS_{78} = 0.833$) are considered as having HS in M_7 and M_8, as predicted in Table 5, Figure 12f.

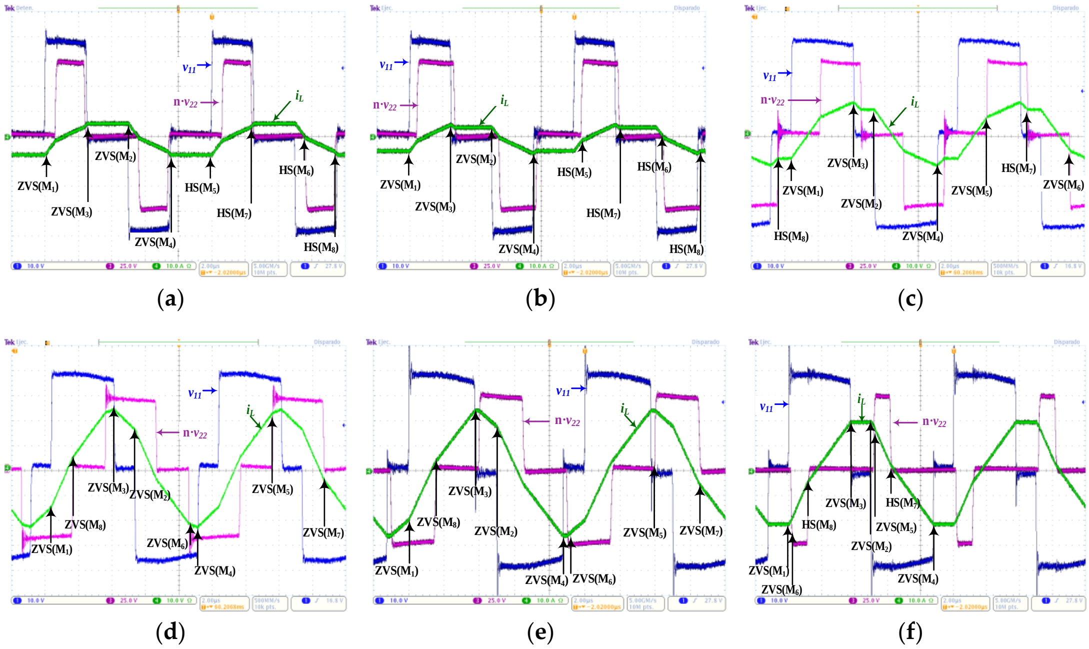

Figure 12. Switching modes for Case I: (**a**) SM_1 with HS in M_5 y M_6 ($\varphi/\pi < SS_{56}$); (**b**) SM_2 with HS in M_5 y M_6 ($\varphi/\pi < SS_{56}$); (**c**) SM_2* with ZVS in M_5 y M_6 ($\varphi/\pi > SS_{56}$); (**d**) SM_3* with ZVS in M_7 y M_8 ($\varphi/\pi > SS_{78}$); (**e**) SM_4 with ZVS in M_7 y M_8 ($\varphi/\pi > SS_{78}$); and (**f**) SM_5 with HS in M_7 y M_8 ($\varphi/\pi < SS_{78}$).

Figure 13 shows six switching modes (SM_1, SM_2, SM_3, SM_4, SM_5, and SM_3*) for Case II and d = 0.677, applying Equation (10) with values $D_1 \leq d$. In this case of study, all the switching modes are likely to achieve ZVS or ZCS except for SM_1 and SM_3*, which may have HS in the Extended Switching Mode, as shown in Table 8 and Figure 10. Figure 13a shows switching mode SM_1, with the Bridge 1 switches in ZVS and those in Bridge 2 in ZCS for D_1 = 0.44, D_2 = 0.664 and φ/π = 0.048. In Figure 13b, the switching mode SM_2 is shown, achieved ZVS in M_3, M_4, M_5, and M_6, and ZCS in M_1, M_2, M_7, and M_8 for D_1 = 0.42, D_2 = 0.656 and φ/π = 0.206. Figure 13c shows four switches with ZCS (M_1, M_2, M_7 and M_8) and four with ZVS (M_3, M_4, M_5 and M_6) for D_1 = 0.132, D_2 = 0.2 and φ/π = 0.458, as detailed in Table 8 for switching mode SM_3. Figure 13d–f show all their switches in ZVS, corresponding to switching modes SM_4 (D_1 = 0.312, D_2 = 0.34 and φ/π = 0.806), SM_5 (D_1 = 0.221, D_2 = 0.435 and φ/π = 0.896), and SM_3*(D_1 = 0.564, D_2 = 0.838 and φ/π = 0.521), respectively.

With these experimental results, the analysis carried out in Sections 3 and 4 and summarised in Table 5 for Case I and Table 8 for Case II, have been validated.

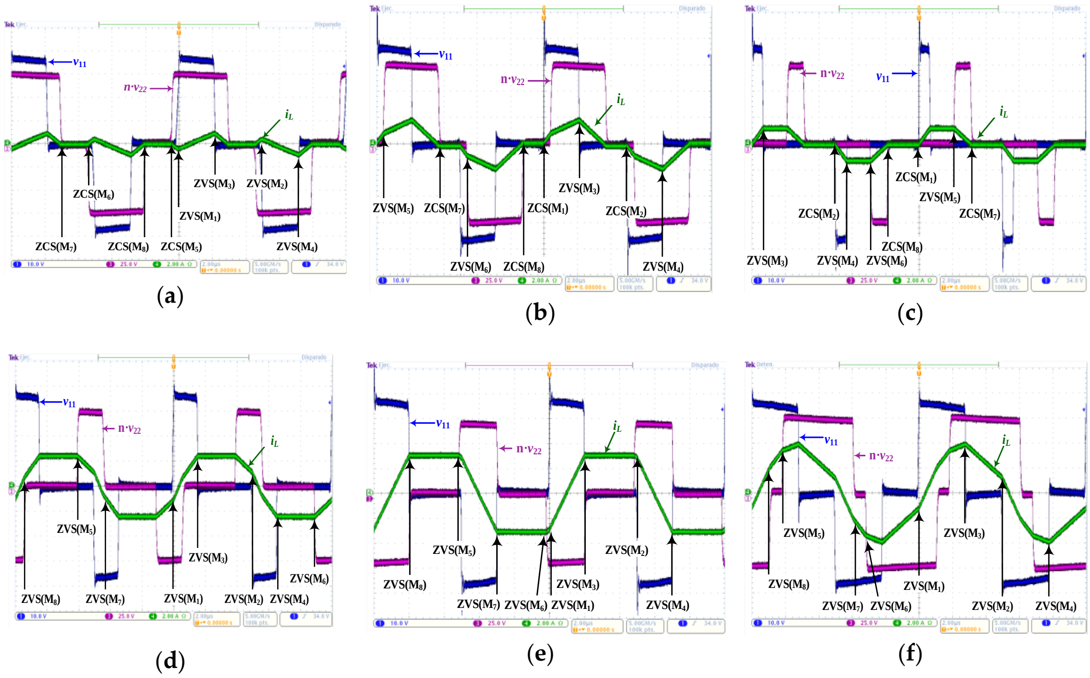

Figure 13. Switching modes for Case II: (**a**) SM_1 for $D_1 = 0.44$, $D_2 = 0.664$, and $\varphi/\pi = 0.048$; (**b**) SM_2 for $D_1 = 0.42$, $D_2 = 0.656$, and $\varphi/\pi = 0.206$; (**c**) SM_3 for $D_1 = 0.132$, $D_2 = 0.2$, and $\varphi/\pi = 0.458$; (**d**) SM_4 for $D_1 = 0.312$, $D_2 = 0.34$, and $\varphi/\pi = 0.806$; (**e**) SM_5 for $D_1 = 0.221$, $D_2 = 0.435$, and $\varphi/\pi = 0.896$; (**f**) SM_3* for $D_1 = 0.564$, $D_2 = 0.838$, and $\varphi/\pi = 0.521$.

6. Conclusions

This paper provides an exhaustive analysis of the different DAB switching modes when TPS, EPS, and PS modulation are applied. This analysis allows the identifying of the best switching modes, among the possible fifty-six different ones, as well as the most suitable combinations of modulation variables to guarantee Zero-Voltage-Switching (ZVS) or Zero-Current-Switching (ZCS), and therefore advance getting the best performance for whole output power ranges and each V_1 and V_2 ratio. With this analysis, it is easier to do further analysis, such as to reduce reactive energy or to define the variables values to get minimum RMS current.

Four cases of study have been established for positive φ, depending on the relative value of input and output voltages and the duty cycle in the bridges voltage waveforms. Two of these four possible cases are considered (Case I and Case II) in this paper since the other two are complementary. Seven switching modes, named as SM_1, SM_2, SM_2*, SM_3, SM_3*, SM_4, and SM_5 have been identified for each case. The analytical expression about boundaries, inductor current and average output power are provided for each analysed switching mode.

The analysis carried out allows knowing the switching in each switch (ZVS, ZCS or HS), detailed in Tables 5 and 8 for Case I and Case II, respectively. This information is essential to quantify the power losses in each switch (both switching and conduction losses) and to improve the efficiency and the power density of the converter. Some of the most relevant conclusions regarding the soft-switching are the following:

- In Case I, only three (SM_3*, SM_4 and SM_5) of the seven switching modes can achieve ZCS or ZVS for all the switches, although the only SM_3^* has a minimum inductor RMS current when $D_1 > 0.5$. The remaining switching modes (SM_1, SM_2, SM_2*, and SM_3) operate with hard switching in a leg of bridge 2, since $\varphi < SS_{56}$ (D_1, D_2) or $\varphi < SS_{78}$ (D_1, D_2), see Table 5, Figure 8d,f.
- In Case II, ZVS and ZCS are reached for all switching modes and the whole power range. For low and medium powers, soft switching is got by applying the expression in Equation (10) with $D_1 \leq d$ and $D_2 < 1$. High power is got either by operating in extending mode with $D_2 = 1$ and

$D_1 > d$ (EPS modulation), or with D_2 = 1 and D_1 =1 (PS modulation). For SM_1, SM_2, and SM_2*, the lowest RMS current is obtained at the boundary between them, see Figure 10d for the same transferred power. For the highest power, SM_3* achieves the lowest inductor RMS current.

A 250 W DAB experimental prototype has been built and tested in the laboratory to validate the theoretical analysis and the soft-switching conditions for the switching modes of Case I and Case II. In addition, the switching in each switch has been verified, for each switching mode.

Author Contributions: C.C. did theoretical analysis, derivation, circuit implementation, experimental testing, data processing and wrote the original draft paper. A.B. is the responsible for funding acquisition, supervision and administration, her contributions were related with the theoretical analysis, data analysis, and the paper reviewing and editing. A.R. wrote and reviewed the paper. P.A. contributed with theoretical analysis and with significant comments on the manuscript structure. A.L., C.F. and P.Z. reviewed and contributed with useful comments on the paper structure and mains paper contributions.

Funding: This research was funded by the Spanish Ministry of Economy and Competitiveness and ERDF, grant number DPI2014-53685-C2-1-R.

Acknowledgments: This work has been partially supported by the Spanish Ministry of Economy and Competitiveness and FEDER (ERDF), through the research project "Storage and Energy Management for Hybrid Electric Vehicles based on Fuel Cell, Battery and Supercapacitors"-ELECTRICAR-AG-(DPI2014-53685-C2-1-R).

Conflicts of Interest: The authors declare no conflicts of interest.

Nomenclature

V_1	DC voltage for bridge 1.	d	Voltage ratio.
V_2	DC voltage for bridge 2.	v_{gx}	Gate-source voltage for Mosfet "x".
v_{11}	Output voltage of the Bridge 1.	SM_x	Switching mode "x".
v_{22}	Input voltage of the Bridge 2.	M_x	Switch "x".
D_1	Pulse width of v_{11}.	SS_{xy}	Soft switching condition for MOSFET "x" and "y".
D_2	Pulse width of v_{22}.	DAB	Dual Active Bridge.
φ	Phase shift between v_{11} and v_{22}.	PS	Phase shift.
fsw	Switching frequency.	SPS	Simple Phase Shift.
Tsw	Switching period.	DPS	Dual Phase Shift.
n	Transformer turns ratio.	TPS	Triple Phase Shift.
L	Series inductor.	EPS	Extended Phase Shift.
i_L	Inductor current.	ZVS	Zero voltage switching.
V_L	Inductor voltage.	ZCS	Zero current switching.

References

1. Yu, F.; Cao, S.; Xie, Y.; Wheeler, P. Study on bidirectional-charger for electric vehicle applied to power dispatching in smart grid. In Proceedings of the 2016 IEEE 8th International Power Electronics and Motion Control Conference, Hefei, China, 22–26 May 2016.
2. Evzelman, M.; Ur Rehman, M.M.; Hathaway, K.; Zane, R.; Costinett, D.; Maksimovic, D. Active Balancing System for Electric Vehicles With Incorporated Low-Voltage Bus. *IEEE Trans. Power Electron.* **2016**, *31*, 7887–7895. [CrossRef]
3. Xue, L.; Shen, Z.; Boroyevich, D.; Mattavelli, P.; Diaz, D. Dual Active Bridge-Based Battery Charger for Plug-in Hybrid Electric Vehicle with Charging Current Containing Low Frequency Ripple. *IEEE Trans. Power Electron.* **2015**, *30*, 7299–7307. [CrossRef]
4. Mastromauro, R.A.; Poliseno, M.C.; Pugliese, S.; Cupertino, F.; Stasi, S. SiC MOSFET Dual Active Bridge converter for harsh environment applications in a more-electric-aircraft. In Proceedings of the 2015 International Conference on Electrical Systems for Aircraft, Railway, Ship Propulsion and Road Vehicles (ESARS), Aachen, Germany, 3–5 March 2015.
5. Tariq, M.; Maswood, A.I.; Gajanayake, C.J.; Gupta, A.K. A Lithium-ion battery energy storage system using a bidirectional isolated DC-DC converter with current mode control for More Electric Aircraft. In Proceedings of the 2016 IEEE Symposium on Computer Applications & Industrial Electronics (ISCAIE), Batu Feringghi, Malaysia, 30–31 May 2016.

6. Khan, M.M.S.; Faruque, M.O. Management of hybrid energy storage systems for MVDC power system of all electric ship. In Proceedings of the 2016 North American Power Symposium (NAPS), Denver, CO, USA, 18–20 September 2016.
7. Xie, R.; Shi, Y.; Li, H. Modular multilevel DAB (M^2DAB) converter for shipboard MVDC system with fault protection and ride-through capability. In Proceedings of the 2015 IEEE Electric Ship Technologies Symposium (ESTS), Alexandria, VA, USA, 21–24 June 2015.
8. Rico-Secades, M.; Calleja, A.; Llera, D.G.; Corominas, E.L.; Medina, N.H.; Miranda, J.C. Cosine Phase Droop Control (CPDC) for the Dual-Active Bridge in lighting smart grids applications. In Proceedings of the 2016 IEEE International Conference on Industrial Technology (ICIT), Taipei, Taiwan, 14–17 March 2016.
9. Yin, C.; Wu, H.; Locment, F.; Sechilariu, M. Energy management of DC microgrid based on photovoltaic combined with diesel generator and supercapacitor. *Energy Convers. Manag.* **2017**, *132*, 14–27. [CrossRef]
10. Fathabadi, H. Novel wind powered electric vehicle charging station with vehicle-to-grid (V2G) connection capability. *Energy Convers. Manag.* **2017**, *136*, 229–239. [CrossRef]
11. Pires, V.F.; Romero-Cadaval, E.; Vinnikov, D.; Roasto, I.; Martins, J.F. Power converter interfaces for electrochemical energy storage systems—A review. *Energy Convers. Manag.* **2014**, *86*, 453–475. [CrossRef]
12. De Bernardinis, A. Synthesis on power electronics for large fuel cells: From power conditioning to potentiodynamic analysis technique. *Energy Convers. Manag.* **2014**, *84*, 174–185. [CrossRef]
13. Amin, A.; Shousha, M.; Prodic, A.; Lynch, B. A transformerless dual active half-bridge DC-DC converter for point-of-load power supplies. In Proceedings of the 2015 IEEE Energy Conversion Congress and Exposition (ECCE), Montreal, QC, Canada, 20–24 September 2015; pp. 133–140.
14. Alonso, A.R.; Sebastian, J.; Lamar, D.G.; Hernando, M.M.; Vazquez, A. An overall study of a Dual Active Bridge for bidirectional DC/DC conversion. In Proceedings of the 2010 IEEE Energy Conversion Congress and Exposition, Atlanta, GA, USA, 12–16 September 2010; pp. 1129–1135.
15. Zhao, B.; Yu, Q.; Sun, W. Extended-Phase-Shift Control of Isolated Bidirectional DC–DC Converter for Power Distribution in Microgrid. *IEEE Trans. Power Electron.* **2012**, *27*, 4667–4680. [CrossRef]
16. Wen, H.; Su, B. Operating modes and practical power flow analysis of bidirectional isolated power interface for distributed power systems. *Energy Convers. Manag.* **2016**, *111*, 229–238. [CrossRef]
17. Lei, T.; Wu, C.; Liu, X. Multi-Objective Optimization Control for the Aerospace Dual-Active Bridge Power Converter. *Energies* **2018**, *11*, 1168. [CrossRef]
18. Sun, C.; Li, X. Fast Transient Modulation for a Step Load Change in a Dual-Active-Bridge Converter with Extended-Phase-Shift Control. *Energies* **2018**, *11*, 1569. [CrossRef]
19. Oggier, G.G.; GarcÍa, G.O.; Oliva, A.R. Switching Control Strategy to Minimize Dual Active Bridge Converter Losses. *IEEE Trans. Power Electron.* **2009**, *24*, 1826–1838. [CrossRef]
20. Liu, X.; Zhu, Z.Q.; Stone, D.A.; Foster, M.P.; Chu, W.Q.; Urquhart, I.; Greenough, J. Novel Dual-Phase-Shift Control With Bidirectional Inner Phase Shifts for a Dual-Active-Bridge Converter Having Low Surge Current and Stable Power Control. *IEEE Trans. Power Electron.* **2017**, *32*, 4095–4106. [CrossRef]
21. Malek, M.H.A.B.A.; Kakigano, H. Fundamental study on control strategies to increase efficiency of dual active bridge DC-DC converter. In Proceedings of the IECON 2015—41st Annual Conference of the IEEE Industrial Electronics Society, Yokohama, Japan, 9–12 November 2015; pp. 1073–1078.
22. Calderon, C.; Barrado, A.; Rodriguez, A.; Lazaro, A.; Fernandez, C.; Zumel, P. Dual active bridge with triple phase shift by obtaining soft switching in all operating range. In Proceedings of the 2017 IEEE Energy Conversion Congress and Exposition (ECCE), Cincinnati, OH, USA, 1–5 October 2017; pp. 1739–1744.
23. Calderon, C.; Barrado, A.; Rodriguez, A.; Lazaro, A.; Sanz, M.; Olias, E. Dual active bridge with triple phase shift, soft switching and minimum RMS current for the whole operating range. In Proceedings of the IECON 2017—43rd Annual Conference of the IEEE Industrial Electronics Society, Beijing, China, 29 October–1 November 2017; pp. 4671–4676.
24. Chakraborty, S.; Tripathy, S.; Chattopadhyay, S. Minimum RMS current operation of the dual-active half-bridge converter using three degree of freedom control. In Proceedings of the 2016 IEEE Energy Conversion Congress and Exposition (ECCE), Milwaukee, WI, USA, 18–22 September 2016; pp. 1–8.
25. Harrye, Y.A.; Ahmed, K.; Adam, G.; Aboushady, A. Comprehensive steady state analysis of bidirectional dual active bridge DC/DC converter using triple phase shift control. In Proceedings of the 2014 IEEE 23rd International Symposium on Industrial Electronics (ISIE), Istanbul, Turkey, 1–4 June 2014; pp. 437–442.

26. Huang, J.; Wang, Y.; Li, Z.; Lei, W. Unified Triple-Phase-Shift Control to Minimize Current Stress and Achieve Full Soft-Switching of Isolated Bidirectional DC–DC Converter. *IEEE Trans. Ind. Electron.* **2016**, *63*, 4169–4179. [CrossRef]
27. Xiong, F.; Wu, J.; Hao, L.; Liu, Z. Backflow power optimization control for dual active bridge DC-DC converters. *Energies* **2017**, *10*, 1403. [CrossRef]
28. Krismer, F.; Kolar, J.W. Closed form solution for minimum conduction loss modulation of DAB converters. *IEEE Trans. Power Electron.* **2012**, *27*, 174–188. [CrossRef]
29. Everts, J. Closed-Form Solution for Efficient ZVS Modulation of DAB Converters. *IEEE Trans. Power Electron.* **2017**, *32*, 7561–7576. [CrossRef]
30. Riedel, J.; Holmes, D.G.; McGrath, B.P.; Teixeira, C. Maintaining Continuous ZVS Operation of a Dual Active Bridge by Reduced Coupling Transformers. *IEEE Trans. Ind. Electron.* **2018**, *65*, 9438–9448. [CrossRef]
31. Zhao, B.; Song, Q.; Liu, W.; Sun, Y. Dead-Time Effect of the High-Frequency Isolated Bidirectional Full-Bridge DC–DC Converter: Comprehensive Theoretical Analysis and Experimental Verification. *IEEE Trans. Power Electron.* **2014**, *29*, 1667–1680. [CrossRef]
32. Li, J.; Chen, Z.; Shen, Z.; Mattavelli, P.; Liu, J.; Boroyevich, D. An adaptive dead-time control scheme for high-switching-frequency dual-active-bridge converter. In Proceedings of the 2012 Twenty-Seventh Annual IEEE Applied Power Electronics Conference and Exposition (APEC), Orlando, FL, USA, 5–9 February 2012; pp. 1355–1361.
33. Xu, F.; Zhao, F.; Shi, Q.; Wen, X. Researches on the Output Power Range of ZVS of Dual Active Bridge Isolated DC-DC Converters. In Proceedings of the 2018 IEEE Transportation Electrification Conference and Expo, Asia-Pacific (ITEC Asia-Pacific), Bangkok, Thailand, 6–9 June 2018; pp. 1–5.